Science, Engineering and Technology Vol. 5, No. 1, pp. 248-273
www.setjournal.com *https://doi.org/10.54327/set2025/v5.i1.150*

Complementary Machining – Machining Strategy for Surface Modification: A Review

Thabo Nelson Mathonsi[1], Rudolph Frans Laubscher[1]

[1]*University of Johannesburg, Cnr Barry Hertzog and Napier Road, Richmond, Johannesburg, Auckland Park, 2006, PO Box 524, South Africa.*

Abstract

All fabrication techniques utilized to manufacture metallic parts modify the surface integrity of the part. Complementary machining is a relatively recent machining strategy characterized by combining metal cutting and mechanical surface treatment. Typically, it implies that after conventional machining, the cutting insert is used reversely to modify the surface by local plastic deformation. To improve product performance, mechanical surface treatment is an additional phase in the manufacturing process chain that usually results in longer production times and higher costs. As a result, a variety of hybrid techniques have been created, such as complementary machining, which has the benefit of using conventional machine tools and their associated cutting tools. The study on complementary machining is reviewed in the article. The main focus is to assess the viability of complementary machining to modify surface integrity for enhanced properties by specifically establishing its effect on tool wear, surface roughness, microhardness, fatigue, microstructure, and residual stress state.

Keywords: *Surface engineering, surface integrity, complementary machining, surface treatment, cutting-edge geometry.*

1. Introduction

A component's desired forms can be produced within specified dimensional tolerances and surface quality standards using a variety of manufacturing techniques used in industry. The most important surface integrity parameters that are imparted by tools employed extensively in machining processes, and particularly for their finishing versions, are surface topography and texture [1]. In the sense that the proper manufacturing technique must be applied in order to get good functionally oriented surfaces, this needs to be looked at from two perspectives: the process control and the tribological function. The management of related texture types produced by different processes presents an opposing issue, too. The latter and the machine tools must both improve as a result of these techniques.

Since the dawn of machining, the characterisation and analysis of engineering-surface texture have created a perplexing metallurgical problem that remains unsolved to date. Furthermore, when considering high-precision or functional performance requirements [2], the complexity of surface textures necessitates a comprehensive description both globally and at various levels. Surface texture has historically been utilized more as an indicator of process variation due to damaged machining elements, machine tool vibrations, tool wear, and other factors than as a gauge of machined component performance [1]. In industrial practice, a reliable method and the specification of the arithmetic average R_a, were deemed enough.

New production tolerances have been imposed by evolving technological advancements, but a thorough understanding of tribological phenomena suggests the necessity of functional surface characterization, which would lead to an increase in parameters [2].

Several studies have been carried out in the literature to provide a succinct and precise description of surface

Corresponding author: *Thabo Nelson Mathonsi (tmathonsi@uj.ac.za)*
Received: *19 June 2024*; Revised: *4 October 2024*; Accepted: *14 October 2024*; Published: *5 November 2024*

texture, with a particular focus on the connection between profile characteristics and manufacturing process factors [2]. Surface topology, or the arrangement of textures according to their shapes, has been the subject of a thorough examination into the potential of several manufacturing research objectives. The following factors determine how difficult it is to achieve the necessary surface quality [3]:

- The the connection between the necessary surface function and surface quality;
- Choosing the production process and putting the ideal process parameters into practice; and
- The the assessment of appropriate representative surface properties.

The majority of modern technologies rely on the unique characteristics of certain solids for their processes to operate satisfactorily. These qualities are primarily bulk properties. These characteristics, however, are superficial characteristics for a crucial class of occurrences. Because its surface should perform several engineering roles in a range of difficult settings, this is important for wear-resistance components [4]. The behavior of a material is influenced by its surface, contact area, and operating environment. A field of study known as *surface science* has developed to completely comprehand surface characteristics and they effects on the operation of different parts, apparatuses, and machines.

Simply put, the outermost layer of an entity is called its surface. The transition layer between two or more entities that differ in any or both of their physical or chemical characteristics is referred to as an interface [4]. Any system with abrupt changes in density, crystal structure, orientation, chemical composition, and ferro- or para-magnetic ordering is said to have a surface or interface, according to Hudson [5]. Riviere [6] and Walls [7] discovered that high-resolution microscopy, along with physical and chemical techniques, can be used to closely investigate surfaces and interfaces. This insight led to the development and application of numerous testing devices, ranging from basic to quite complex. In order to satisfy their natural interest about surface and interface contact phenomena, humans have created these tools.

Any type or degree of surface and interface interaction between two or more things can be studied within the field of surface science. Physical, chemical, electrical, mechanical, thermal, biological, geological, astronomical, and even emotional connections are all possible [8]. The classification of a number of significant regions within the various surface science topics is displayed in Figure 1.

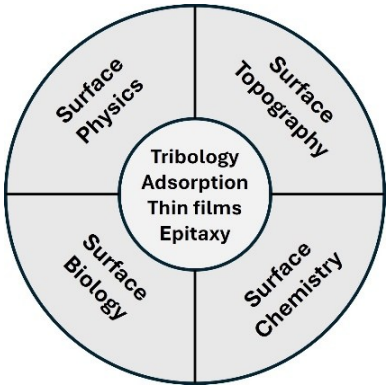

Figure 1. Important areas of surface science [4].

Surface engineering has existed for as long as people have used structural materials. From ancient times to the early 1970s, humanity has continuously developed surface engineering, often without consciously recognising the concept [9]. One of the most crucial methods for differentiating engineering goods based on their quality, performance, and life-cycle cost is surface engineering. The design of the surface and substrate as a functionally graded system to produce cost-effective performance improvements that neither component could achieve alone is known as surface engineering, and it has been used for more than ten years [4]. This activity is very multidisciplinary by definition (Figure 2).

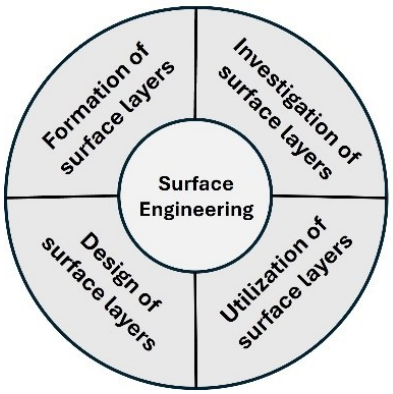

Figure 2: Important areas of surface engineering [4].

Managers in a variety of industry sectors are realizing more and more that the effective use of surface engineering requires an integrated strategy at the design stage that involves cooperation between surface and design engineers. The multidisciplinary field of surface engineering aims to improve the serviceability of

engineering components by customizing their surface characteristics. The *ASM Handbook* defines *surface engineering* as the "treatment of the surface and near-surface regions of a material to allow the surface to perform functions that are distinct from those functions demanded from the bulk of the material"

The multidisciplinary field of surface engineering aims to improve the serviceability of engineering components by customizing their surface characteristics. Surface engineering is the "treatment of a material's surface and near-surface regions to allow the surface to perform functions that are distinct from those demanded from the bulk of the material," according to the ASM Handbook [9]. King [10] states that the goal of surface engineering is to produce components with the following desired qualities or attributes:

- Enhanced resistance to corrosion by means of the sacrificial protection or barrier;
- Enhanced resistance to oxidation and/or sulfidation;
- Enhanced resistance to wear;
- Decreased losses of friction energy;
- Better mechanical qualities, including increased toughness, hardness, or fatigue life;
- Enhanced electrical or electronic characteristics;
- Enhanced insulation against heat;
- Enhanced biological characteristics; and
- Enhanced visual appearance.

Geometric characteristics like surface roughness and waviness, together with metallurgical physical features like microhardness, residual stress, and microstructure changes, are the fundamental determinants of surface integrity, a crucial parameter for assessing the surface and subsurface quality of components [11].

In their publication: *A new need for surfaces formed by material removal procedures*, published in the 1960s, Field and Kahles [12] first proposed the idea of surface integrity. They then gave an outline of how machining affects surface integrity [13]. A minimum, standard, and extended data set were proposed as criteria for evaluating data, and the majority of the work on surface integrity evaluation techniques was completed in the 1970s [14]. This idea was once further advanced in 1989 by Tagazawa [15] through more in-depth investigation and substantial testing.

According to research, a component's fatigue performance, wear resistance, and corrosion resistance are all directly impacted by surface integrity [16]. Novovic et al. [17], for instance, assessed how machined topology and integrity affected fatigue life. The findings demonstrated that longer fatigue life is the outcome of low roughness values. According to Kalisz et al. [18], high compressive stress and high hardness can work together to provide excessive wear resistance. According to Amanov et al. [19], AISI 304 specimens have a longer fatigue life when their compressive residual stress is increased.

According to research, a component's fatigue performance, wear resistance, and corrosion resistance are all directly impacted by surface integrity [16]. Novovic et al. [17], for instance, assessed how machined topology and integrity affected fatigue life. The findings demonstrated that longer fatigue life is the outcome of low roughness values. According to Kalisz et al. [18], high compressive stress and high hardness can work together to provide excessive wear resistance. According to Amanov et al. [19], AISI 304 specimens have a longer fatigue life when their compressive residual stress is increased. Srinvasan et al. [20] a machined surface containing a significant amount of microhardness is usually associated to a longer fatigue life as well as a lower wear rate and coefficient of friction.

Peng et al. [11] classified factors that influence surface integrity into three main categories:

1. cutting parameters: cutting speed, feed rate and depth of cut;
2. tool parameters: tool wear, texturing, material and geometry; and
3. cooling conditions: cooling medium, pressure and distance.

Chen and Jawaid [21] looked into how titanium's surface integrity was affected by machining. The findings indicated that the roughness and microhardness of the machined surface tended to increase when titanium alloys were processed using uncoated carbide cutting tools, high cutting speeds, and feed rate. Sun et al. [22] evaluated the surface integrity of titanium under end milling conditions. The results showed an increase in surface roughness as a result of the high feed rate. Furthermore, it has been noted that improvements in cutting speed are correlated with increases in the machined surface's hardness and

roughness. Ozel [16] found that low cutting speeds and feed rates should be implemented when machining titanium alloys

Liang and Wang [23] and Khanna et al. [24] confirmed that tool performance is also a significant factor influencing surface integrity. A study on tool wear behaviour by Liang and Liu [25] showed that a titanium workpiece machined using fresh tools resulted in low surface roughness as compared to those machined using worn-out tools. Worn-out tools have been reported to result in a thicker plastic deformation layer [27], higher microhardness [28], and greater surface roughness [26] [29] compared to fresh tools. Additionally, they cause the residual stress to shift from compressive to tensile [30].

Astakhov [4] discovered that a number of flaws that compromise surface integrity are created and caused during part manufacture. They can be divided into two categories: manufacturing flaws and original material defects. The most frequent flaws discovered in practice are as follows:

- Sharply defined interior or exterior separations are called cracks. Microcraks are those that cannot be seen with unaided eye without a magnificantion of 10x or greater
- Phase transformations, re-crystallization, alloy depletion, decarburzation, and molten and re-cast, re-solidfied, or re-deposited material, as in electrical discharge machining, are examples of microstructural changes brought on by temperature and high contact pressures in metallurgical transformation.
- Temperatures, deformations, and process forces all contribute to residual stresses.
- Shallow depressions are called craters.
- The metal's inclusions are tiny, non-metallic components or compounds.
- The weakening of grain boundary due to corrosion or liquid-metal embitterment is known as an intergranular attack.
- Pis are shallow surface depressions that are typically cased by physical ir chemical attacks.
- In manufacturing, plastic deformation is a servere surface distortion brought on by high pressures from friction or tools.

Various components in the manufacturing process require surface modification treatments, which can enhance service properties such as fatigue resistance, tribological performance, and corrosion resistance [31]. Thermal, thermo-mechanical, or mechanical surface treatments can be used to achieve these objectives. The latter, which cause plastic deformation of the surface and material layers beneath it, shall be referred to as surface-modification processes from here on. Additionally, this causes a number of properties in this component region to change. Smoothing, geometric texturing, work hardening, compressive-residual stresses, or microstructural alterations like phase transition could be the primary characteristics of the surface modification process.

Usually, a few of these impacts can happen at the same time, although at varying intensities. Jawahir et al. [26], for instance, discovered that geometrical changes will happen as a result, affecting the entire workpiece.

The traditional technique known as mechanical-surface treatment (MST) was first used when artisans forged helmets and swords while they were being shaped. The manufacture of weapons in the shape of gun barrels is also where the first use in the new period began [27]. But it may also have anything to do with the manufacturing of railroad axles and bearing bolts.

Surface modification techniques such as shot peening (SP) [28], surface mechanical attrition treatment (SMAT) [29], laser shock peening (LSP) [30], [31], and ultrasonic surface hardening [32] have been used to improve the mechanical properties of components, including wear resistance, fatigue life, and surface hardness. These improvements are distinguished by excessive density dislocations, refined grains, and high-strain rate plastic deformation brought on by severe impacts to the surfaces, which leave compressive residual stress in both the surface and subsurface regions.

Figure 3 displays the schematics of the previously discussed surface altering techniques. Balls, usually made of metal, glass, or ceramic, are used in SP and SMAT to bombard a component, dimpling the surface and causing shock waves and local plastic deformation in the materials, as seen in Figure 3(a). By employing high-energy-density, short-duration laser pulses to ablate a protective layer on a component's surface, LSP creates quickly expanding plasma. Metal undergoes plastic deformation due to a shock wave produced by the

expanding plasma confined between the surface and a clear confinement layer (Figure 3(b)). In ultrasonic surface hardening, a needle with a fixed tip or a rolling ball is moved to strike the surface at an ultrasonic frequency using an electro-mechanical ultrasonic transducer to generate ultrasonic vibrations (Figure (3c)).

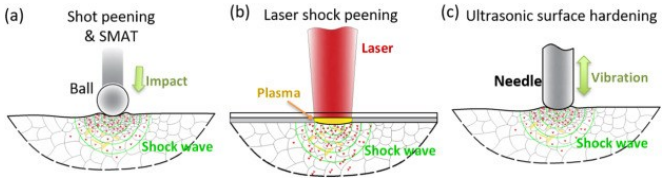

Figure 3. Ilustrations showing the three different of surface hardening methods: (a) SP and SMAT; (b) LSP; and (c) ultrasonic surface hardening [33].

Ultrasonic nanocrystal surface modification (UNSM), ultrasonic impact treatment (UIT), and ultrasonic surface rolling processing (USRP) are among the devices that operate on this concept.

The technique known as shot peening (SP), which was first developed on Tilgham's patent in the 1870s, uses an unguided tool and discontinuous surface contact [34]. Sand that had been pressurized by centrifugal forces, steam, or air was used. As additional industrial uses developed and this approach improved from the 1920s to the 1940s, fatigue fatigue [35] [36] [37], stress-corrosion cracking, and corrosion fatigue [38] were all improved. Because it works well with components with intricate designs and thin walls, the SP process is regarded as one of the most popular and successful MSTs for aero-engine applications [39]. Investigating surface integrity features under SP treatment circumstances has attracted a lot of attention in recent years. For instance, Liu et al. [40] assessed the impact of SP pressure and time on the surface integrity properties of titanium alloys in collaboration with Xie et al. [41] [42]. The results showed that SP intensity increases surface roughness, compressive residual stress, and microhardness. Wu et al. [43] evaluated the impact of shot material, diameter, and SP intensity on the surface properties of titanium alloy. The findings showed that a ceramic shot with a diameter of 1.08 mm and a peening intensity of 0.18 mm produces the best SP conditions. The characteristic curve of the residual stress field in titanium was examined by Li et al. [44] [45] for wet SP.

Ultra surface rolling (USR), a mechanical surface treatment technique, has garnered a lot of attention lately. Static rolling and dynamic ultrasonic vibrations are used in the USR method to produce a smooth microhardness on the target surface [46] [47]. A rolling tool installed on the spindle of the computer numerical center (CNC) machining center is typically used for this procedure. In this procedure, the air-pressurized, ultrasonic vibrating rotatable rolling ball rolls and strikes the component surface [48]. Numerous investigations on this method focused on how it affected mechanical properties, gradient microstructure, fatigue characteristics, and surface integrity. The fatigue behavior of titanium alloys under ultrasonic impact treatment was examined by Dekhtyar et al. [49]. They discovered that titanium alloys treated under ultrasonic impact conditions had a much higher fatigue strength than untreated ones because of their increased surface integrity. Similarly, Liu et al. [50] discovered that the USR method produced significant lifetime improvements because of enhanced surface quality, work hardening, residual stress, and refined grains in the microstructure. The gradient crystalline structure of TC11 alloys under the USR process was examined by Zhao et al. [51], who discovered that a plastically deformed layer around 70 μm thick was produced with an improved fatigue strength in comparison to the untreated specimens.

The LSP is a new and advanced MST technology that generates shock waves with high amplitudes (GPa), high energy (GW/cm2), ultra-short pulse widths (nanoseconds), and ultra-high strain rates (10-7s-1). During the LSP process, the ablating layer—typically black tape—sticks to the target surface and absorbs laser light. Instantaneous creation and vaporization of a high-temperature (>107 °C) and high-pressure (GPa) plasma occurs. Significant plastic deformation is caused by high-pressure shock waves that propagate into the material's subsurface when a transparent layer, typically running water, stops the plasma detonation wave [52] [53].

The mechanical characteristics, impact on surface integrity, fatigue characteristics, and microstructure of titanium alloys following LSP procedures have all been experimentally determined in a number of research conducted in recent years. For instance, Cellard et al. [54], assessed how LSP process parameters affected work hardening, surface topology, and residual stress for Ti-17. The findings showed that LSP process parameters have negligible effect on surface topology, no effect on work hardening, and a major impact on residual stresses. The

effects of LSP on TC17 alloy blades were examined by Zou et al. [55] and Qiao [56], who observed a notable improvement in microhardness and compressive residual stresses as well as the induction of high-density dislocations and refined grains, which improved fatigue life.

In the last few years, several studies have focused on experimentally determining the mechanical properties, influence on surface integrity, fatigue properties and microstructure of titanium alloys after LSP processes. Cellard et al. [54], for example, evaluated the influence of LSP process parameters on residual stress, surface topology and work hardening for Ti-17. The results revealed that LSP process parameters have a significant influence on residual stresses, a minimal influence on work hardening, and no influence on surface topology. Zou et al. [55] and Qiao [56] investigated the effects of LSP on TC17 alloy blades, noting significant improvement in the microhardness and compressive residual stresses while inducing high-density dislocations and refined grains, thereby improving fatigue life.

The mechanical characteristics, impact on surface integrity, fatigue characteristics, and microstructure of titanium alloys following LSP procedures have all been experimentally determined in a number of research conducted in recent years. For instance, Cellard et al. [54] assessed how LSP process parameters affected work hardening, surface topology, and residual stress for Ti-17. The findings showed that LSP process parameters have negligible effect on surface topology, no effect on work hardening, and a major impact on residual stresses. Zou et al. [55] and Qiao [56], investigated the effects of LSP on TC17 alloy blades and found that the induction of high-density dislocations and refined grains, along with a significant improvement in microhardness and compressive residual stresses, improved fatigue life.

Burnishing, on the other hand, relies on a tool's constant, directed contact with the material's surface. Burnishing was found to be associated with an increase in fatigue strength by Foppl and Heydekampf [57]. When Thum and Wiegand [58] statistically correlated burnishing and its impact on fatigue strength, they found similar results.

2. Complementary Machining

Several surface-modification methods have been created in recent years that are directly comparable to the technologies outlined above. Complementary machining is a new surface modification process in addition to the well-known ones like shot peening [27]. One method for quickly mechanically treating the surface of metallic workpieces is complementary machining [59]. The main feature of complementary machining is that the cutting tool is used to perform a mechanical surface treatment following machining. The cutting tool creates an elastic-plastic deformation in the surface layer by moving across the workpiece surface in the opposite direction of the machining process.

Immediately following the machining process, the complementary machining process strategy combines machining with the reversal of the cutting insert for a mechanical-surface change [60]. Significant plastic deformation is created on the surface layer during this operation because of the reverse-machining orientation, which could lead to grain refinement. In Figure 4, the contact conditions for this complementary machining are displayed.

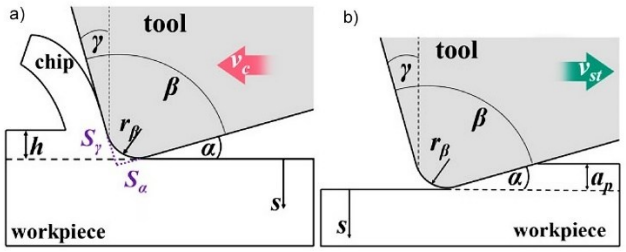

Figure 4. Complementary machining contact conditions include: a) machining and b) mechanical surface modification [60].

Orthogonal cutting is the basis for the nomenclature for machining, whereas mechanical surface modification is based on mechanical-surface treatment. During complementary machining, the process forces and maximum temperature are significantly impacted by the state-of-the-art microgeometry employed [60]. The resulting surface layer's states are thus greatly influenced by the state-of-the-art microstructure. However, a key obstacle in creating this process strategy is still designing a state-of-the-art microgeometry that can sustain the thermo-mechanical stress spectrum and that influences the surface layer states appropriately [60]. Although the creation of nanocrystalline surface layers is made feasible

by the state-of-the-art microgeometry, it is probable that the thermo-mechanical stress would influence this cutting edge and cause premature tool wear.

1.1. Cutting edge microgeometry

The angles and slopes of the cutting tools' edges and salient forces at their cutting sites are referred to as tool geometry [61], and are shown in Figure 5. The American National Standard B94.50-1975 [62] and ISO Standard 3002/1 [63] are the two fundamental standards that cutting tool geometry complies with. Similar cutting tool geometry is defined by both standards, while the reference planes and notations differ significantly. Numerous angles and surfaces defined in several planes are included in tool geometry [64]. The work surface, which is the first surface of a workpiece that will be removed during the machining process, and the machined surface, which is the last surface of the machined workpiece, are the two fundamental surfaces that must be taken into account during machining, per ISO 3002/1. Therefore, it is essential to determine how cutting angles affect any output metrics that can be assessed in this account. The following describes the angles that are thought to be important during complementary machining and that could affect the surface finish [65].

1.1.1. Back rake angle

The rear rake angle, measured in a perpendicular plane across the side cutting edge, is the angle created by the face of the single point cutting tool and a line parallel to the tool's base. Depending on the direction of the slope, this angle could be either positive or negative. When the slope face is facing uphill, the rear rake angle is positive; when it is facing downward, the back rake angle is negative. Chips are easier to remove from the workpiece at this angle.

1.1.2. Side rake angle

The side rake angle is the angle at which the face of the tool is tilted sideways. It is located between the surface of the flank immediately below the point and the line that descends from the point perpendicular to the base. When allowing space between the workpiece and the tool is required to avoid the workpiece rubbing against the tool's end flake, the side rake angle is taken into account.

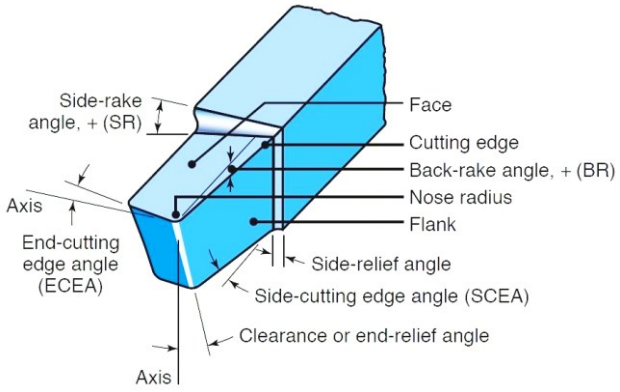

Figure 5. Schematic illustration of single point cutting tool [65].

1.1.3. Front clearance/back relief angle

The angle at which the tool's face tilts sideways is known as the side rake angle. It lies between the line that descends from the point perpendicular to the base and the surface of the flank just below the point. The side rake angle is considered when it is necessary to leave room between the workpiece and the tool to prevent the workpiece from rubbing against the tool's end flake.

2.1.1 Side clearance/relief angle

The angle that separates the section of the side flank directly below the side edge from a line perpendicular to the tool's base and at right angles to the side is known as the relief angle. As the tool pierces the material, it helps to avoid interference. Its purpose is to create relief between the tool's flank and the workpiece's surface.

2.1.2 Wedge/Lip angle

The angle that separates the face from the flank is known as the lip angle. When the clearance and rake angle are at their lowest, the wedge angle is at its highest. Work on hard materials and a great depth of cut are made possible by a larger wedge angle.

2.1.3 Tool signature of single point cutting tool

Tool angles can be easily specified by using a standardized, condensed system called "Tool Signature" [66] (see Figure 6). The angles that a tool employs when

cutting are shown by this method. Additionally, it stipulates that the tool's active angles must be normal to the cutting edge. There is a catch, though: the system will only function properly if the tool shank is positioned perpendicular to the workpiece axis.

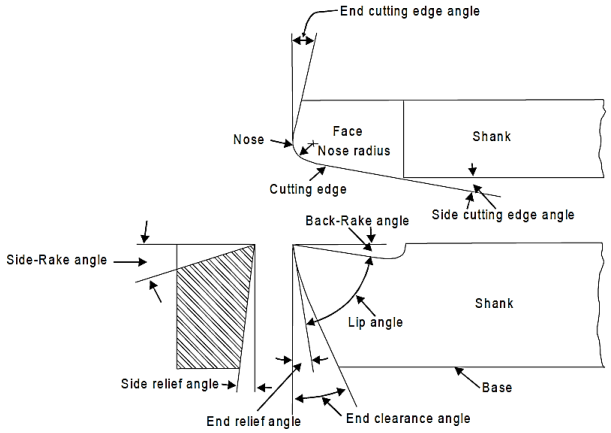

Figure 6. Elements of tool signature [66].

Seven elements comprise the signature of a single point cutting tool, always stated in the following manner [66]:

1. back rake angle (0°)
2. side rake angle (7°)
3. end relief angle (6°)
4. side relief angle (8°)
5. end cutting edge angle (15°)
6. side cutting edge angle (16°)
7. nose radius ($0.8\ mm$).

Typically, a tool signature only lists the numerical values of each component in the single point cutting tool, such as 0-7-6-8-15-16-0.8, omitting the symbols for degrees and millimeters.

In the manufacturing sector, high productivity particularly the high dependability of machining techniques is crucial [67]. According to these requirements, one element that significantly affects tool life and the quality of a machined surface is the cutting edge's microgeometry. Cutting pressures, heat distribution, tool wear, surface roughness, residual stresses, and machining process stability are all impacted by the cutting edge's design.

2.2. Cutting edge geometry

To establish the influence of cutting-edge microgeometry during machining, it is essential to understand the microgeometry's design. Denkena et al. [68, 69, 70] and Wyen and Wegener [71] established the edge treatment description approach by defining four fundamental parameters (see Figure 7): δ_α, δ_γ, Δr and φ. Both symmetrical and asymmetrical cutting edges are possible. Form-Factor:

$$K = \frac{\delta_\gamma}{\delta_\alpha}$$

Where:

K = Form-Factor;

δ_γ = Cutting edge segment on the rake face; and

δ_α = Cutting edge segment on the flank face.

The form-factor describes the direction of the profile slope towards the rake face $(K > 1)$ or flank face $(K < 1)$.

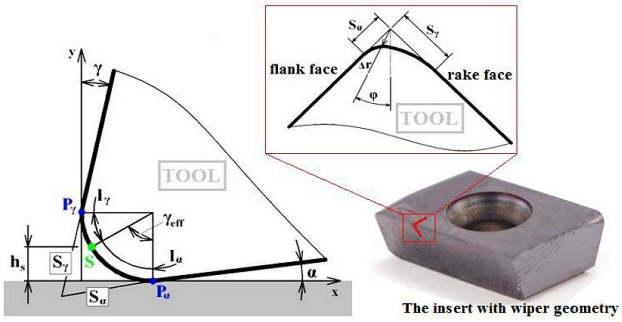

Figure 7. Characterisation of the cutting-edge micro-geometry [68].

With regard to symmetric rounding $(k = 1)$, the edge radius (r_β) will be utilised instead δ_γ and δ_α. There are different types of microgeometry depending on the type of insert chosen, as seen in Figure 8: symmetric rounding, K = 1.0, with $r_\beta = 30\mu m$ and asymmetric rounding; K = 2.0, with Sγ =60 µm and δ_α =30µm, which are prepared plunge-face grinding and by brushing [69, 70].

As presented in Figure 8, microgeometries are characterised by the cutting-edge section at the rake face δ_γ and the cutting-edge section at the flank face δ_α.

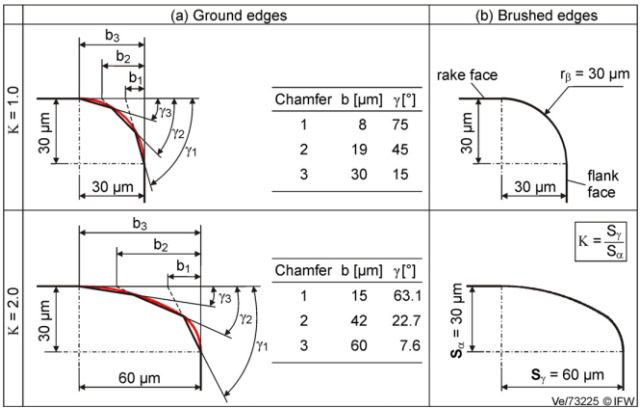

Figure 8. Cutting edges that have been discretized using plunge-face grinding (a) and continuously rounded using brushing (b) [72].

The optimal cutting-edge microgeometry for complementary machining was discovered by Zanger et al. [60] The thermomechanical strain on the cutting tool and the ensuing grain refinement in the surface layer were investigated. Three distinct form-factors were examined: K = 0.2, K = 1, and K = 2. During the experiment, a test bench similar to the one reported by Puls et al. [73, 74] was employed. Using an AISI 4140, quasi-orthogonal cutting tests were carried out on a MAG 5-axis mill-turn machine. The cutting tools were uncoated, and the initial cutting-edge radius was r_β = 40±10 mm, with the z cutting wedge angle set at 90°. 100 m/min was the same velocity used for complementary machining and machining. The machining depth of cutting, however, was different from the complementary machining depth, which was ∂_c = 120 μm and $\partial_{c,st}$ = 20 μm, , respectively. The form-factor technique of Denkena et al. [70] was used to characterize the cutting-edge microgeometry, and it included a description of the average cutting-edge rounding S.

2.2.1 Nanocrystalline surface layer

The impact of microstructure on the surface layers for complementary machining was investigated throughout the experiment (Figure 9). As far out as 2.41 μm from the surface d_s, a nanocrystalline surface layer is visible. The bulk material with a grain size of d_g > 1 µm comes after this layer, which is followed by a microcrystalline sheared layer.

Following complementary machining, the thickness s_{gr} of the grain refined surface layers with a nanocrystalline microstructure is shown in Figure 10.

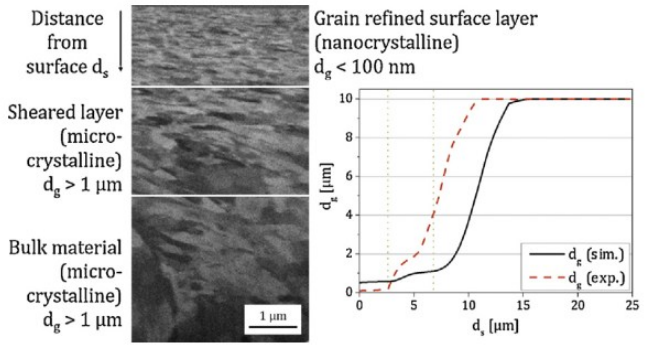

Figure 9. Examined the surface layer following complementary machining (using the form-factor K = 2 to cut the edge microgeometry) [60].

According to Segebade et al. [75], cutting edges with a form-factor of K < 1 can be used to achieve the thickest post-machining nanocrystalline surface layers. Less obvious nanocrystalline surfaces are produced when cutting edges with a form-factor of K > 1 are used.

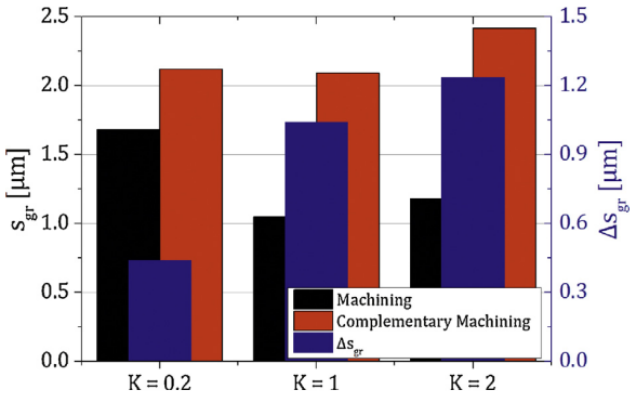

Figure 10. Thickness of the nanocrystalline surface layer that results from complementary and machining [60].

Complementary machining, however, can help with this. Nanocrystalline surface layers with a large and less variable thickness are produced by complementary machining. Only the application of a cutting edge with a form-factor K = 2 produces a marginally perceptible thickness.

2.2.2 Thermo-mechanical load on cutting edge

The thermo-mechanical load at the cutting edge-workpiece contact face was examined using a FEM simulation. The temperature distribution at the tool during machining and related operations is displayed in Figure 11(a). Plotting of the findings from the surface analysis of Figure 12 as a function of distance along the tool surface is depicted in Figure 11(b).

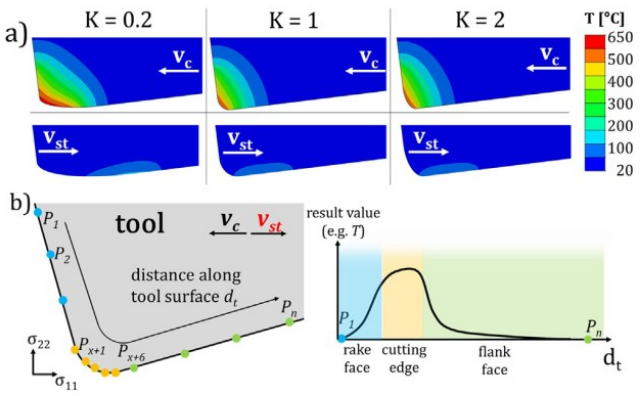

Figure 11. Process temperatures T at the tool (a) and schematic depiction for analysing the tool surface (b) [60].

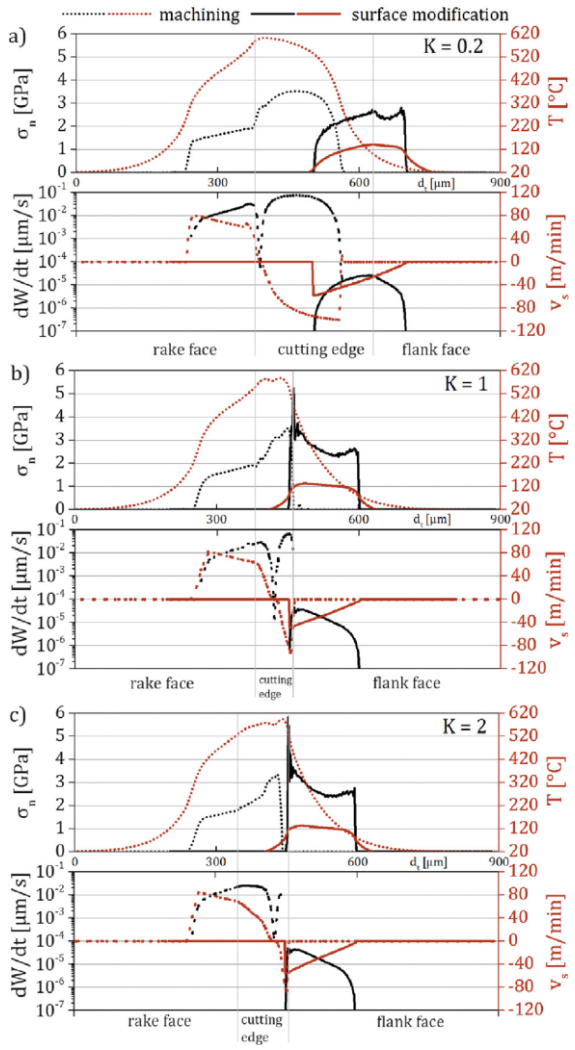

Figure 12. Thermomechanical stress($\boldsymbol{\sigma_n}$, T), that results from machining and mechanical surface modification, sliding velocity vs predicted wear rate (dW/dt), and form-factors K = 0.2 (a), K = 1 (b), and K = 2 (c) [60].

In addition to the results presented in Figure 12, the change of microgeometries of the cutting edge was also evaluated for both machining and complementary machining. Figure 13 illustrates how the form-factor ΔK and the average cutting-edge rounding $\Delta\bar{S}$ change for both machining and complementary machining when compared to the original cutting-edge microgeometries. Following machining, the form-factor K dropped and the average cutting edge rounding changed, resulting in a negative change in the form-factor ΔK for both form-factors K = 1 and K = 2. All of the cutting edges got dull as a result. The use of uncoated cutting tools was the cause of this. The average cutting-edge rounding changed just slightly for complementary machining.

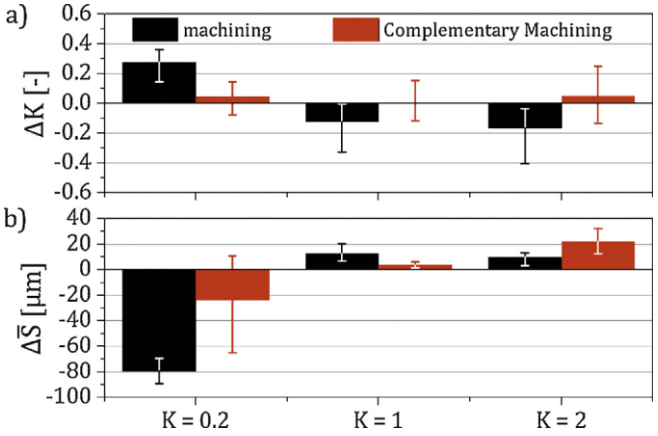

Figure 13. Change of form-factor $\Delta\boldsymbol{K}$ (a) and resulting average cutting-edge rounding $\Delta\bar{\boldsymbol{S}}$ (b) [60].

Together with the findings shown in Figure 12, an assessment of the cutting edge's microgeometries was conducted for both machining and complementary machining.

Figure 13 illustrates how the form-factor ΔK and the average cutting-edge rounding $\Delta\bar{S}$ change for both machining and complementary machining when compared to the original cutting-edge microgeometries. Following machining, the form-factor K dropped and the average cutting edge rounding changed, resulting in a negative change in the form-factor ΔK for both form-factors K = 1 and K = 2. All of the cutting edges got dull as a result. The use of uncoated cutting tools was the cause of this. The average cutting-edge rounding changed just slightly for complementary machining. However, there was an increase in the change of form-factor ΔK when compared to machining for both form-factor K = 1 and K = 2.

2.3. Influence of complementary machining parameters

The effect of advanced microgeometry on temperature and process forces, as well as process-induced surface layer grain refinement, was examined by Gerstenmeyer et al. [76] during the complementary machining of Armco-Iron and AISI 4140. Two scenarios were used in the experimental effort to determine how form-factor K affected the surface layer states that resulted. The penetration depth $\partial_{c,st}$ was kept constant at 20 µm for scenario 1, but the surface modification velocity v_{st} fluctuated between 20 and 150 m/min. In this situation, the maximum temperatures and consequent grain size for AISI 4140 were used to determine how surface modification velocity affected the process forces. In the second scenario, the penetration depth varied between 10 µm and 40 µm, but the surface modification velocity was kept constant at 150 m/min. Both Armco-Iron and the AISI 4140 were examined in the second scenario. Furthermore, based on r_β = 40 µm, three distinct microgeometries of K = 0.2, 1, and 2 were examined.

2.3.1 Penetration depth

The surface modification force F_{st} and passive force F_p for the various surface modification velocities and form-factor K for a penetration depth of 20 µm are shown in Figure 14 and Figure 15.

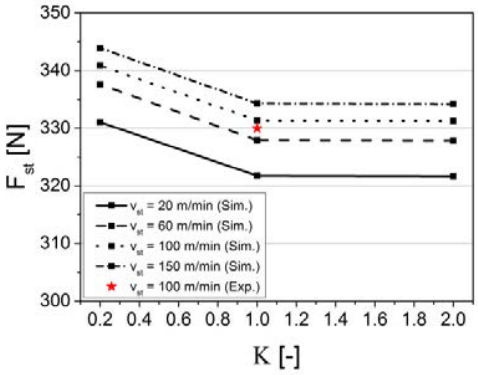

Figure 14. Surface modification force for 20 µm penetration depth and surface modification velocities for AISI 4140 [76].

The outcomes were consistent with those of Gerstenmeyer et al. [77] and Zanger et al. [60]. Surface modification velocities affect process forces. The findings validated that process forces rise when form-factor K is less than 1. Denkena et al. [72] reported a similar finding, stating that a dull cutting edge produces greater process forces than a sharp edge. Form-factors K < 1 are considered dull cutting-edge microgeometry for complementary machining, while K > 1 are considered sharp. Process forces differ significantly between these two types of cutting edges, with an enhanced form-factor having no effect on the process forces.

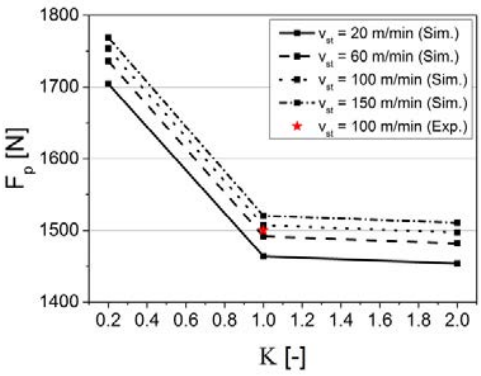

Figure 15. For AISI 4140, passive force is required for surface modification velocities and penetration depths of 20 µm [78].

Figure 16 displays the heat produced during complementary machining for form-factors K = 0.2 and 2 with a penetration depth of 20 µm. The results showed that, in contrast to form-factor K < 1, which raises the temperature of a larger volume of material, form-factor K > 1 produced local concentrated temperatures.

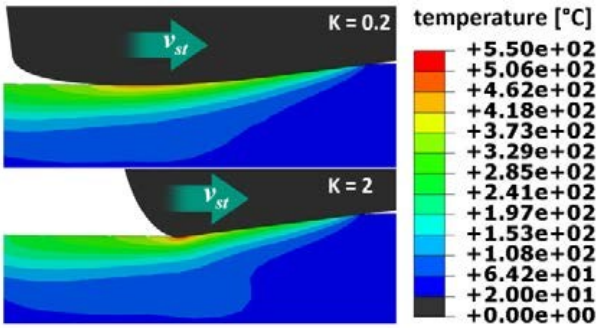

Figure 16. Temperature T of penetration depth of 20 µm and surface modification velocity of 150 m/min for AISI 4140 [76].

The highest temperature for ∂_p = 20 μm with various surface modification velocities for AISI 4140 is shown in Figure 17. The findings showed that form-factor K and temperature were directly correlated, with an increase in form-factor leading to an increase in temperature. significant temperatures were also a result of significant surface modification velocities. This resulted from the impact of surface modification velocity on the model's two heat sources, plastic deformation and friction. With

high surface modification velocity, both sources increased.

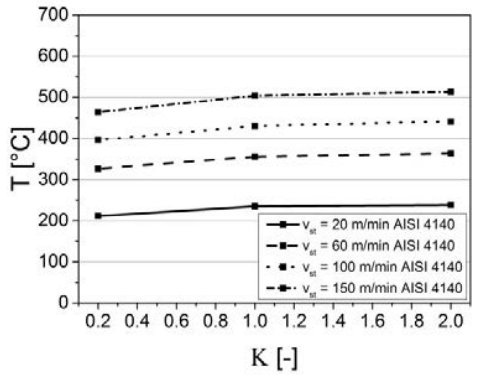

Figure 17. Maximum temperature T for AISI 4140 penetration depth of 20 µm and surface modification velocities [76].

Following surface modification by complementary machining, the resulting grain size, g_s is displayed in Figure 18 in relation to the initial state. The findings indicate that temperature has a significant impact on grain refining. Only high surface modification velocities (v_{st} > 100 m/min) result in notable grain refinement, as Figure 18 illustrates. This is why the second simulation series used simulations with a constant surface modification velocity v_{st} = 150 m/min. There was variation in the penetration depth (∂_p).

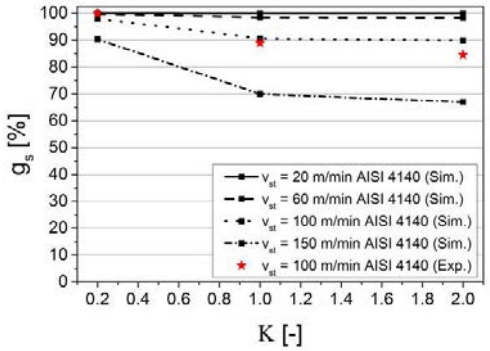

Figure 18. For surface modification velocities and penetration depth $(\boldsymbol{\partial_p})$ of 20 µm for AISI 4140, the grain size is $\boldsymbol{g_x}$ [76].

2.3.2 Surface modification velocity

Figure 19 and Figure 20 display the process force for Armco-Iron for a range of form-factors, penetration depths, and surface modification velocity of 150 m/min. The results clearly show that, for Armco-Iron, form-factor has no discernible effect on process forces under complementary machining circumstances. However, with AISI 4140, process forces increased as penetration depth increased. Higher passive forces were produced by a form-factor of K < 1 for the passive force than by a form-factor of K < 1. The region impacted by the passive force expanded as a result of the larger contact area.

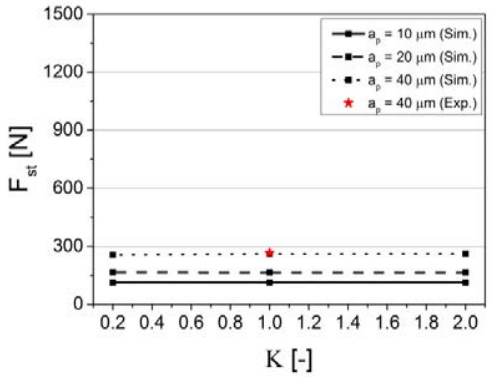

Figure 19. Surface modification force for Armco-Iron at varying penetration depths and a constant surface modification velocity of 150 m/min [76].

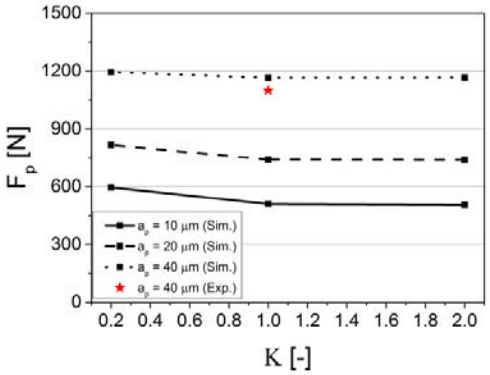

Figure 20. Passive force for varying penetration depths $\boldsymbol{\partial_p}$ for Armco-Iron and a constant surface modification velocity of 150 m/min [76].

2.3.3 Form-Factor

The process force results from Armco-Iron's complementary machining followed a similar pattern to AISI 4140 (Figure 21 and Figure 22). These findings clearly show that the surface modification force is not significantly impacted by the form-factor. On the other hand, form-factor K > 0.2 data showed that passive force might be reduced. For K > 1, however, this remained constant. Armco-Iron's complementary machining showed a similar pattern, albeit AISI 4140 is more vulnerable to the effects of different form-factors.

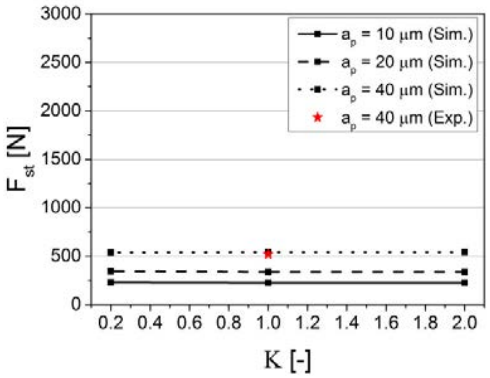

Figure 21. Surface modification force for AISI 4140 at different penetration depths and a constant surface modification velocity of 150 m/min [76].

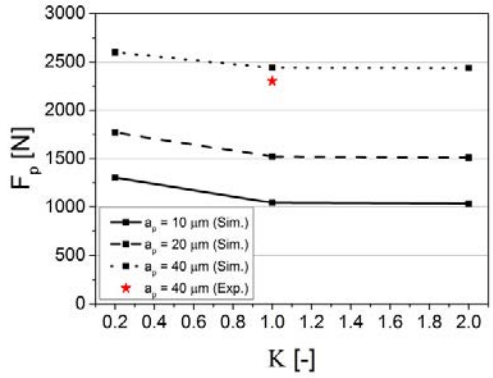

Figure 22. Passive force for AISI 4140 at varying penetration depths and a constant surface modification velocity of 150 m/min [76].

In comparison to Armco-Iron, the process forces obtained during the complementary machining of AISI 4140 were twice as high. These outcomes are consistent with those of [77], which was caused by Armco-Iron's higher ductility and lower strength in comparison to AISI 4140.

Figures 23 and 24 display the maximum temperatures for the different form-factors as well as the penetration depths for Armco-Iron and AISI 4140 at a surface modification velocity of 150 m/min. The findings show that higher plastic deformation at high penetration depths results in higher temperatures. Remarkably, low passive forces and a higher thermal load were obtained with a form-factor of K > 2. High passive forces and a lower thermal load were noted for form-factor K < 1. A significant amount of heat was produced under complementary machining settings because AISI 4140 required more mechanical work than Armco-Iron. This is because AISI 4140's great strength caused plastic deformation, which produced a considerable amount of heat.

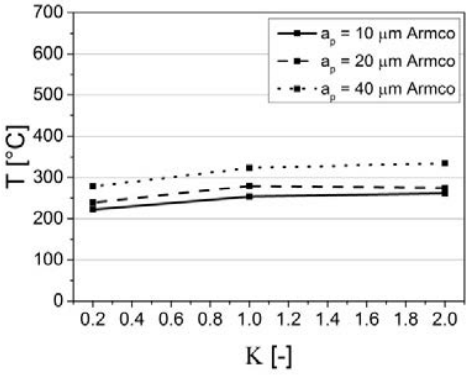

Figure 23. Maximum temperature for Armco-Iron at different penetration depths and a constant surface modification velocity of 150 m/min [76].

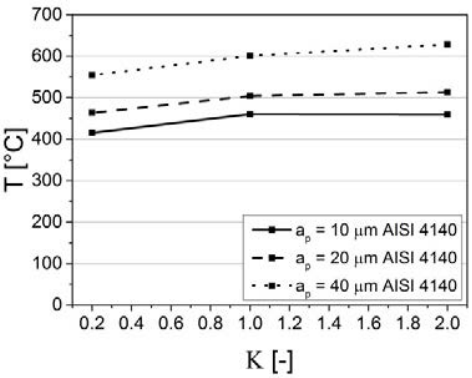

Figure 24. Maximum temperature for AISI 4140 at different penetration depths and a constant surface modification velocity of 150 m/min [76].

Figure 25 displays the resultant grain refinement in AISI 4140 surface treatment for different form-factors (0.2 and 2), surface modification velocity of 150 m/min, and penetration depth of 40 µm. The findings shown that lower grain sizes can be achieved with equal penetration depth and surface treatment velocity for form-factor K > 1.

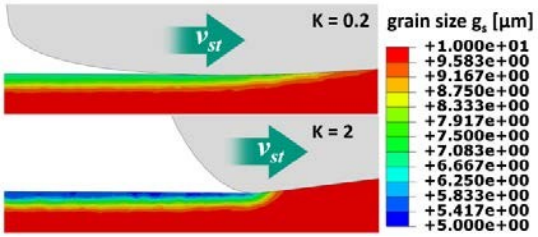

Figure 25. Penetration depths of 40 µm for AISI 4140, grain size data for form-factor K = 0.2 and 2, and surface modification velocity of 150 m/min [76].

The resulting grain refinement for different form-factors and penetration depths is displayed in Figure 26. The results show insignificant grain refinement, which is probably because Armco-Iron's surface modification was

carried out at much lower temperatures than AISI 4140. Temperature has a major impact on grain refining, as was previously seen under the specified limits. Temperatures are higher for form-factor K > 1 than for K < 1. As a result, the grain size gets smaller. Lower temperatures and, as a result, less grain refinement are obtained because form-factor K < 1 generates less heat through plastic straining.

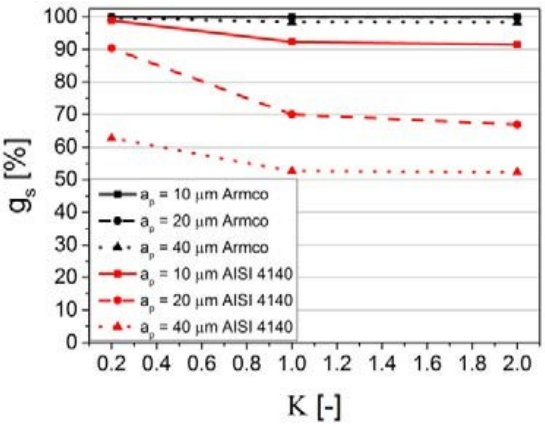

Figure 26. The final grain size is determined by the beginning grain size for AISI 4140 and Armco-Iron at different penetration depths and a constant surface modification velocity of 150 m/min. [76].

2.4. Effects of complementary machining on output parameters

2.4.1 Tool wear

Tool wear, as described by ISO 3685 (1993): Tool-life testing with single-point turning tools, is a gradual degradation of tool material or deformation that causes a tool to alter shape during cutting [63]. Tool wear significantly affects not just tool life but also the final product's quality in terms of surface integrity and dimensional accuracy. When it comes to machining materials that are difficult to machine, like titanium, these factors are even more important.

The impact of different tool types on tool wear during AISI 4140 complementary machining was examined by Schwalm et al. [59] Both uncoated and PVD-coated rhombic tools with a nose radius of rn = 0.8 mm and a wedge angle of 90° were employed (Type I). The uncoated tool's initial average cutting edge rounding was $\overline{S}$ = 6.13 ± 3.21 µm, and its initial form-factor K was 0.96 ± 0.31. For this type of coated tool, the form-factor was K = 1.14 ± 0.25 and the first average cutting edge rounding was $\overline{S}$ = 25.14 ± 6.46 µm. Conversely, Type II PVD-coated cutting tools were employed, which had a nose radius of rn = 0.4 mm and a nose angle of 55°. On the rake face of these instruments was a chip former. The following process settings were used: 100 m/min cutting velocity; 10 m/min surface modification; 100 µm cutting depth; 10 µm penetration depth; and 0.16 mm/rev and 0.0045 mm/rev feed rates for the microgeometry and machining. Tensile tension can cause sensitivity because uncoated tool-type I has a slight initial rounding of the edge. Significant friction is created during complementary machining, which imposes tensile forces on the cutting edge. Lubrication assists in decreasing tensile forces on the cutting edge by reducing friction in the cutting zone. Additionally, lubrication can keep the cutting edge from breaking. The uncoated tool-type I's rake face exhibits a notable breakout. There are several minor surface adhesions and no obvious chipping marks on the cutting edge when comparing the three cutting tools.

Figure 27 shows the cutting edges of coated and uncoated tools following complementary machining. During complmentary machining in dry conditions, uncoated tool-typee I failed. Starting at the cutting edge, a significant breakout can be seen on the rake face of the uncoated type I tool. There are only minor surface adhesions and no obvious chipping marks on the cutting edge as compared to the two coated tools.

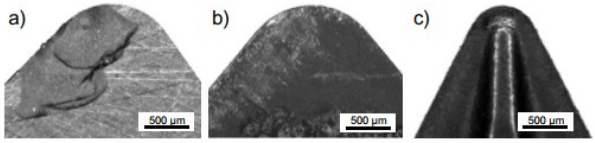

Figure 27. Tool wear following complementary machining can be classified as either a) uncoated type I, b) coated type I, or c) coated type II without lubrication [59].

The brittle nature of the tool is demonstrated by the shell-shaped breakout on the rake face. The tool substrate's edge microgeometry and microstructure may be to blame for this (Figure 28). A type I tool's hardness is greater than that of a type II tool. A type I tool's grain structure is also coarser, according to a direct comparison of the microstructure.

There are no apparent breakouts on the flank side, which comes into continual contact with the workpiece during complementary machining. Compressive stress that does not cause breakouts on brittle cutting materials

is primarily directed to the flank side. Breakouts along the rake side are the outcome of the procedure, which creates tensile strains at the cutting edge.

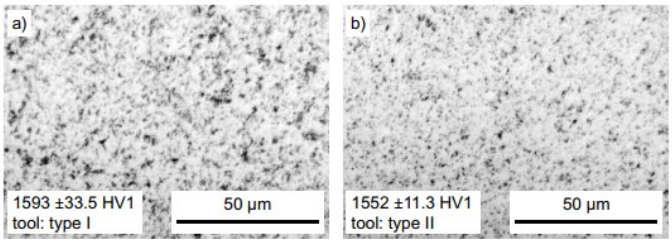

Figure 28. a) Tool-type I and b) tool-type II microstructures [59].

Following complementary machining with uncoated tools under wet cutting conditions, Figure 29 illustrates how the form-factor and cutting-edge rounding changes cause the cutting-edge microgeometry to fluctuate. There are no noticeable changes in the average cutting-edge rounding at a surface treatment velocity of 100 m/min. The average cutting-edge rounding increased at lower surface treatment velocities (10 and 50 m/min). This was explained by the higher adhesion tendency brought on by the friction coefficient and uncoated tool. Tool wear may rise as a result of stick-ship-like effects brought on by the increase in adhesion tendencies.

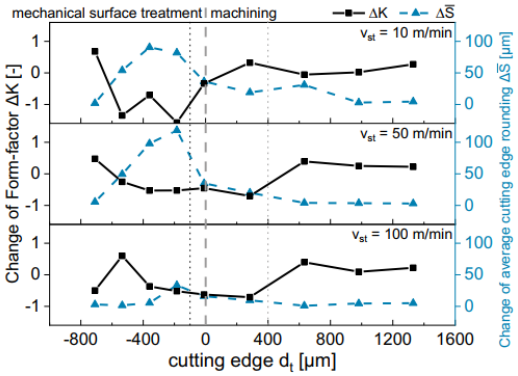

Figure 29. Cutting-edge microgeometry with f_{st} = 0.045 mm/rev and ∂_{st} = 10µm following complementary machining with an uncoated tool-type I in wet cutting circumstances [59].

Figure 30 shows the cutting-edge microgeometry after complementary machining using coated tool-type I under dry cutting conditions (a) and under wet cutting conditions (b). These results prove the observations presented in Figure 28.

As a result of the coatings, minimal tool wear was observed for both complementary machining under wet and dry conditions. In contrast to higher surface treatment velocities, when a slight improvement in cutting-edge microgeometry was found, no appreciable changes in cutting-edge microgeometry were observed at 10 m/min. During complementary machining, the cutting-edge microgeometry changes in the area in contact, as previously observed in Figure 27(a). An increase in surface treatment velocities yields high temperatures. Also, this thermal load on the cutting-edge leads to tool failure, and high temperatures in the cutting zone increase adhesion tendencies and therefore high surface roughness values. This trend is proven by Figure 30(b).

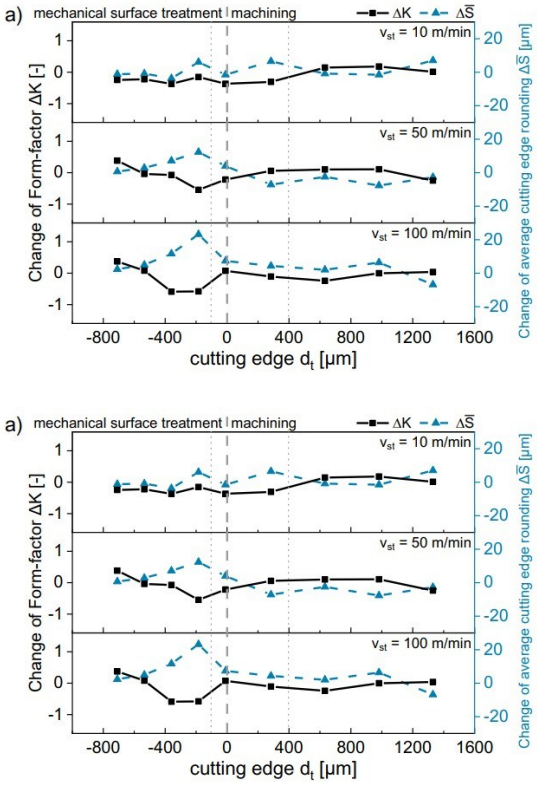

Figure 30. Advanced microgeometry following complementary machining (a) with a coated tool type I without lubrication and (b) with lubrication at a fst = 0.045 mm/rev and ∂_{st} = 10 µm [59].

For 10 m/min, minimal changes to the form-factor and the average edge rounding can be seen. However, when increasing the surface treatment velocity to 100 m/min, a significant change in cutting-edge microgeometry is noticed. The average rounding of the cutting edges increases during machining and complementary machining. In the same dimensions, the form-factor is reduced; this reduction shows wear on the flank face, suggesting that lubrication has no significant impact on wear and its position. There is a possibility that no lubricant will enter the cutting zone due to the high circumferential speed. When compared to complementary

machining in dry cutting circumstances, a modest increase in wear is more noticeable in the machining region. The lubricant's cooling action may be affected in certain circumstances. Conversely, process pressures are raised and thermal softening is reduced. Additionally, cooling causes a high temperature differential at the cutting edge, which puts stress on the substrate. This effect can be linked to an increase in surface roughness levels in addition to tool wear. Zanger et al.'s FE simulations [60] further demonstrated that following machining, the form-factor drops and the average cutting edge rounding rises.

Figure 31 shows the cutting-edge microgeometry after complementary machining with coated tool-type II under dry cutting conditions (a) and wet cutting conditions (b).

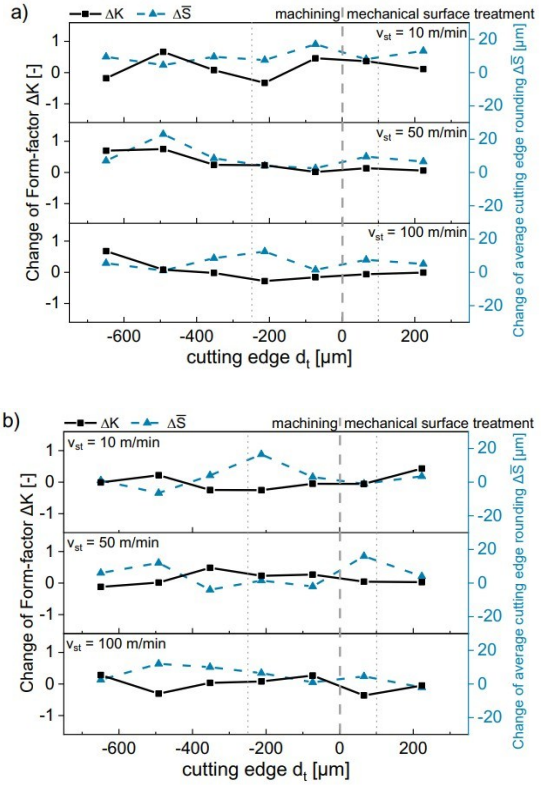

Figure 31. Advancement in microgeometry following complementary machining (a) with coated tool-type II without lubrication and (b) with lubrication at f_{st} = 0.045 mm/rev and ∂_{st} = 10 µm [59].

When comparing the results obtained for tool-type I to those for tool-type II, it is clear that the changes of the average edge rounding and form-factor are not significantly dependent on the change in surface treatment velocity for tool-type II. For tool-type II, the influence of the lubrication on tool wear was minimal.

2.4.2 Surface roughness

In surface engineering, creating high-quality surfaces is a crucial step. Surface roughness affects wear resistance, corrosion protection, fatigue, and the quality and efficacy of succeeding coatings as well as the finish quality of decorative layers.

Schwalm et al. [59] investigated the impact of tool types on surface roughness during complimentary machining. Relevant roughness values for industrial applications, Ra, Rz, and Rt, were tactilely evaluated in the axial direction in compliance with DIN EN ISO 4287 [79]. The results of the roughness values (Ra, Rz, and Rt) after machining are shown in Figure 32. Roughness values were lower when using coated tools for machining than when using uncoated ones. When using tool-type I machining, the coated tool's Ra value was more than 40% higher and its Rz value was 30% lower than that of the uncoated ones. When using tool-type II for machining, a similar finding was seen. Thus, it is evident that during milling, microgeometry affects topography. Surface roughness levels are also influenced by the cutting edge's microgeometry and the condition of the tool surface. It was discovered that the coating on the rake face might lower cutting forces and chip compression by lowering friction in the cutting zone. This results in a more uniform surface by making chip creation easier and facilitating a consistent chip flow. When compared to uncoated tools, this lowers the standard deviation of the Rz and Rt values.

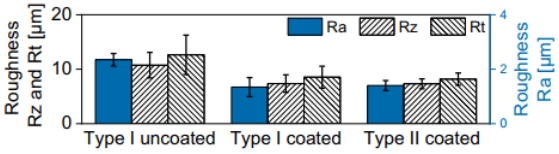

Figure 32. Surface roughness following unlubricated machining at v_c = 100 m/min, f_{st} = 0.045 mm/rev, and ∂_{st} = 100 µm using coated and uncoated tools n [59].

Most notable, however, is the low standard deviation for tool-type II, which incorporates a chip that was previously on the rake face and further promotes simple chip flow. Additionally, the coated tools' first average cutting edge rounding is notably larger. For tool-type I, the coated tool's average cutting-edge rounding is three times higher than the uncoated tool's. Compared to the uncoated tool type I, the coated tool type II has an average cutting-edge rounding that is more than five times higher. The rounding of the cutting edge also affects the topology after machining. Tools with greater edge rounding can

yield improved topology, as demonstrated by Fulemova and Janda [80].

Figure 33(a) displays the surface roughness values that were obtained for complementary machining in dry cutting conditions. The pereentages shown show how complementary machining after machining reduces surface roughness levels. Because of the tool's quick tool wear, no significant results were obtained during the complementary machining utilizing uncoated tool-type I. The absence of results was caused by the inability to process the specimens. For every process parameter, it was discovered that low surface roughness values were achieved during complementary machining. The findings showed that an increase in surface treatment velocity resulted to higher surface roughness values for the coated tool types I and II. This behavior was particularly noticeable for tool-type I, where Ra and Rz values were observed to nearly double as the surface treatment velocity was raised from 10 to 100 m/min. It was discovered that when surface treatment velocities rose, so did standard deviations. The findings of comparing the surface roughness values produced by tool-type I and tool-type II revealed that tool-type I produced somewhat lower roughness values.

Figure 33(b) displays the surface roughness values that were obtained for complementary machining in wet cutting conditions. Uncoated tool-type I could be utilized in these cutting conditions. The tools exhibited nonlinear behavior under wet cutting conditions. The results showed that surface roughness values and standard deviations increased with increasing surface treatment velocities for tool-type I. However, tool-type II showed no discernible difference. Additionally, it was noted that lubrication did not significantly alter the topology of the coated tools. Because of the cutting edge's microgeometry, the process was sensitive to lubrication and surface treatment velocities during the complementary machining with type II tools. Tool-type II achieves a greater deformation gradient in the feed direction than tool-type I because of its smaller nose radius. However, more tool revolutions are needed for tool-type I in order to produce the same surface deformation.

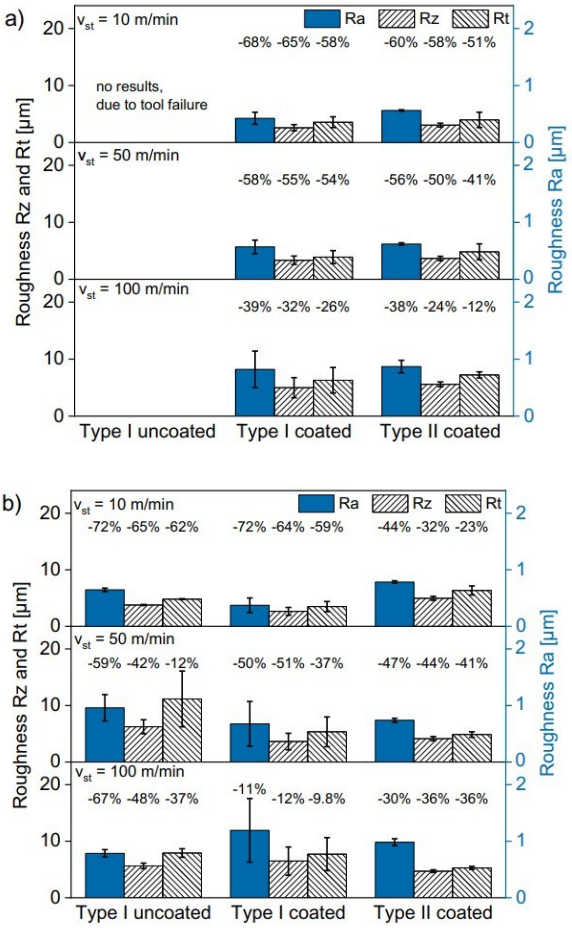

Figure 33. Surface roughness after complementary machining a) without lubrication; and b) with lubrication at fst = 0.045 mm/rev, and ∂st = 10 µm [59].

Gerstenmeyer [78] also investigated the influence of complementary machining on surface roughness. The resulting surface roughness values for machining and complementary machining are illustrated in Figure 34. The results show that the varying feed rated for machining and complementary machining influenced the topology (Figure 34a). The groove spaces generated are in line with the feed rates f_c, and f_{st}. The feed rate used for machining is 3 x larger than that for complementary machining, explaining why the groove spacing $s_{m,c}$ for machining is 3 x larger than the groove spacing $s_{m,st}$ for complementary machining. After complementary machining, the resulting topology was significantly irregular compared to the topology generated during machining. The area roughness S_z is comparable for both machining and complementary machining. Therefore, it can be claimed that because of the abnormalities, the maximum heights are equivalent. Based on the findings, it was determined that complementary machining can cut

the final roughness values in half. Lienert et al. [81] found similar outcomes when they looked into how piezo peening affected surface roughness.

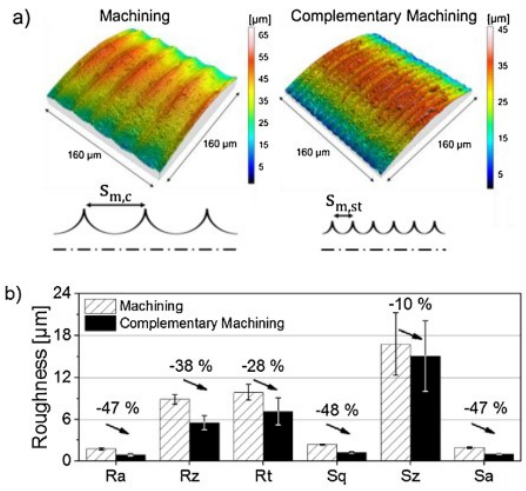

Figure 34. Following machining and complementary machining at v_{st} = 10 m/min, the resulting topography (a) and roughness at v_c = 100 m/min, and f_c = 0.5 mm of AISI4140 [78].

Gerstenmeyer et al. [77] investigated the use of complementary machining as a surface modification strategy. Complementary machining was studied utilizing a brittle material (AISI 4140) and a ductile material (Armco-Iron) in order to gain a better understanding.The cutting speed was kept constant at 100 m/min, while the surface treatment velocity varied from 60 to 100 µm. The depth of cut and the penetration depth was 60 µm and 20 µm, respectively. The resulting surface roughness (R_a and R_z) for AISI 4140 is shown in Figure 35. After the machining was concluded, the surface roughness values were found to have increased slightly compared to the initial values. This increase was soon reduced by the implementation of complementary machining. The surface roughness values were adjusted into the range of R_a = 0.14 µm and R_z = 0.75 µm.

Armco-Iron was also subjected to complementary machining. Figure 36 shows the outcomes of ten repetitions of the surface treatment in these studies. The surface roughness values were found to fall between Ra = 0.86 µm and Rz = 5.8 µm following the initial surface treatment. Surface roughness was reported to be decreased to Ra = 0.18 µm and Rz = 1.11 µm as a result of successive surface treatment repetitions. Plastic deformation in the surface layer was identified as the cause of this decrease in the surface roughness rating. Thus, surface imperfections can be minimized or eliminated. The formation of burrs, which might affect the specimen height, is another effect of repeated surface treatments. This phenomenon was also noticed in [60].

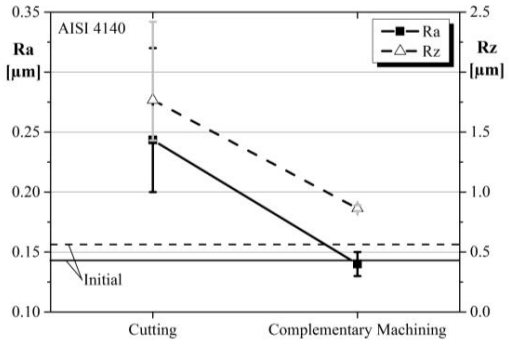

Figure 35. Surface roughness R_a and R_z for AISI 4140 **[77]**.

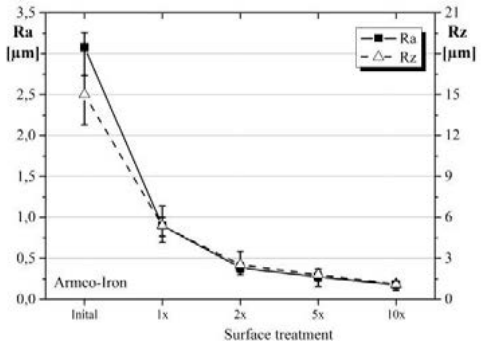

Figure 36. Surface roughness R_a and R_z for Armco-Iron **[77]**.

2.4.3 Microhardness and passive force

Gerstenmeyer et al. [77] also analysed the microhardness HV after complementary machining. The microhardness HV 0.01 at a depth of s = 150 µm below the workpiece surface is represented by the numbers below. The microhardness for the various surface treatment velocities for Armco-Iron is shown in Figure 37. For a v_{st} of 60m/min and a ∂_{pst} of 20 µm, no visible change in microhardness was observed when compared to the initial values. For other penetration depths (5, 10 and 25 µm), microhardness increased up to 104 HV 0.01. For a v_{st} of 100m/min and a ∂_{pst} of 5 µm, the microhardness was constant. The microhardness was found to be 118 HV for 10 µm and 108 HV 0.01 for 20 µm. This was as a result of the plastic deformation process that takes place after complementary machining, resulting in strain hardening of the surface layer.

Based on these outcomes, it is evident that the penetration depth at low surface treatment velocities has minimal influence on microhardness. A significant

change in microhardness was only observed at high surface treatment velocities. However, no change in microhardness was observed for a v_{st} of 100 m/min and a ∂_{pst} of 25 µm when compared to the initial values. This can potentially be attributed to the high rate of plastic deformation and the surface layer's subsequent rise in temperature.

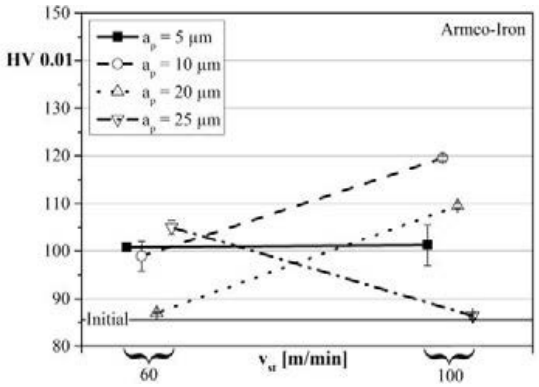

Figure 37. Microhardness HV 0.01 for different surface treatment velocities for Armco-Iron **[77]**.

Figure 38 displays the passive force for Armco-Iron at different surface treatment velocities. The findings indicate that the particular passive force rises with penetration depth. High loads and a significant of plastic deformation were encountered by the surface layer due to high process forces. According to Zanger et al. [82], process temperature rises at the surface layer, reducing flow stress. Armco-Iron and other ductile materials are susceptible to this. Heat-induced softening of a material could be accelerated.

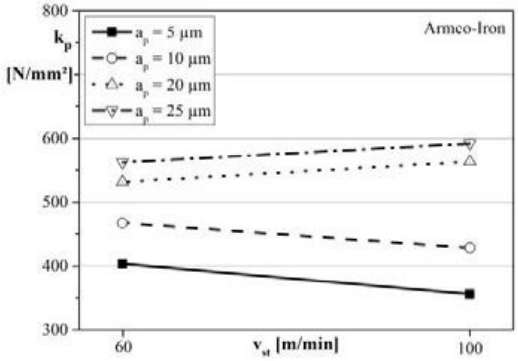

Figure 38. Particular passive force for Armco-Iron at various surface treatment speeds [77].

Figure 39 displays the microhardness for AISI 4140 at different surface treatment velocities. When compared to the initial values, no discernible change in microhardness was seen at a v_{st} of 60 m/min and a ∂_{pst} of 10 µm. The microhardness was found to have reduced from the starting state for ∂_{pst} of 5 µm. There was a small increase in microhardness at penetration depths of 20 µm and 25 µm. There was no discernible change or reduction in microhardness when the surface treatment speed was increased to 100 m/min. Schulze et al. [83], obtained similar results, who established the impact of cutting speed on surface layer microhardness HV. Microhardness HV increased only at a penetration depth of 5 µm. As previously mentioned, the penetration depth causes higher plastic deformation in the surface layer, which raises the process temperature and causes the material to thermally soften. When taking the process forces into account, this softening becomes more apparent.

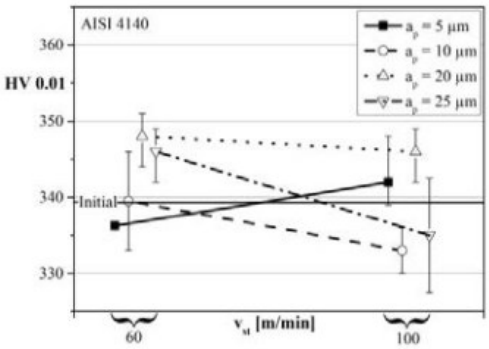

Figure 39. Microhardness HV 0.01 for AISI 4140 at various surface treatment velocities **[77]**.

Figure 40 displays the passive force for Armco-Iron at different surface treatment velocities.

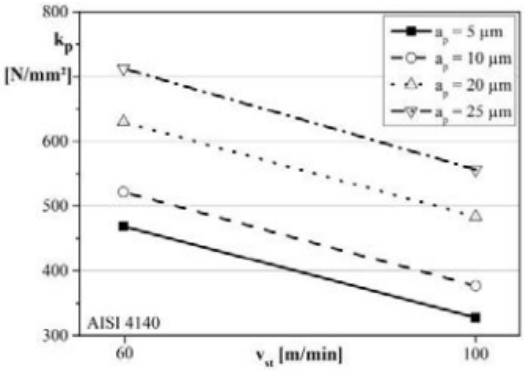

Figure 40. Particular passive force for AISI 4140 at various surface treatment speeds [77].

The findings confirmed that process forces increase in proportion to penetration depth. On the other hand, process forces drop as surface treatment velocity increases. This is consistent with the outcomes of Armco-Iron's complementary machining in [82], but it differs from the outcomes of AISI 4140's complementary

machining in [82]. The decreased penetration depth is one explanation for this discrepancy in outcomes. Additionally, when sliding velocities increase, the coefficient of friction decreases, which explains the declining process force [84].

2.4.4 Fatigue

Tension-compression measurements were performed following both machining and complmentary machining. Figure 41 displays the generated S-Ne curves. The fatigue limit for machining (Figure 41(a)) was recorded at 317 MPa at 5% fracture probability, 374 MPa at 50% fracture probability, and 469 MPa at 95% fracture probability. For machined AISI 4140, these fatigue limits are regarded as modest. Nevertheless, the machined workpiece's surface layer states exhibit low nanocrystalline surface layer, high tensile residual stresses, and substantial surface roughness values, all of which contribute to its poor fatigue strength.

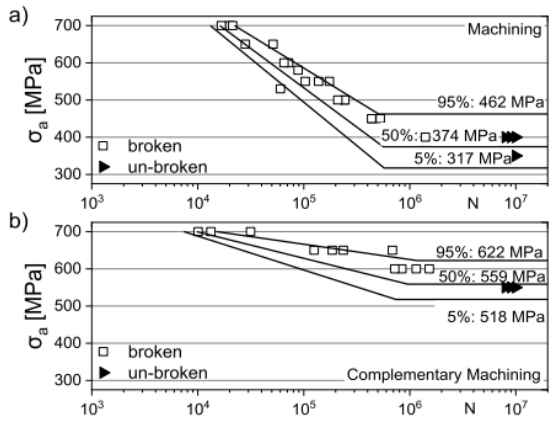

Figure 41. S–N curves and fatigue limits (a) after machining; and (b) after complementary machining [78].

The fatigue limit for complementary machining was 518 MPa at 5% fracture probability, 559 MPa at 50% fracture probability, and 622 MPa at 95% fracture probability. (see Figure 41(b)). A high load amplitude (σ_a = 700 MPa) resulted in a similar fatigue strength for both machining and complementary machining, with the number of cycles between 10^4, and 10^5. The benefits of complementary machining on fatigue are evident in the decrease of load amplitudes. The number of cycles achieved for complementary machining for a load amplitude of σ_a = 650 MPa are between 10^5 and 10^6 whereas machining resulted in a number of cycles lower than 10^5. For load amplitude of σ_a = 600 MPa, a significant improvement in the number of cycles (above 10^6) was achieved for complementary machining, whereas machining could only achieve this number of cycles at a load amplitude of σ_a = 400 MPa. After complementary machining, increases of approximately 63%, 49% and 35% were noticed for a 5%, 50% and 95% probability of fracture, respectively. Surface layer states are improved as a result of the increased fatigue strength. Because of the mechanical surface treatment, the microstructure in the surface layer exhibits a notable grain refinement.

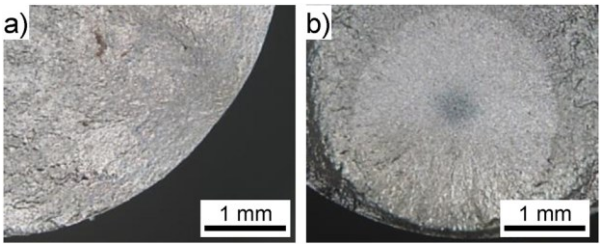

Figure 42. Fractography of (a) a machined; and (b) complementary machined specimen of AISI 4140 [78].

Figure 42 displays a fractography of a machined and complementary machined workpiece. Following complementary machining, a fracture is started beneath the surface for load amplitudes less than σa = 700 MPa. Nevertheless, there was no discernible correlation between the load amplitude and the distance to the surface. Surface cracks appeared for stress amplitudes greater than σ_a = 700 MPa. Therefore, the high load amplitude is not tolerated by surface layer states. For all load amplitudes, the crack was started at the surface during machining. The 5% S-N curve for complementary machining can be compared to the S-N curve of piezo peening, shot peening, and burnishing in order to characterize these results in accordance with earlier studies on fatigue strength [81].

Figure 43 shows a comparison of the various 5% S–N curves for different mechanical surface treatment processes (piezo peening, shot peening, burnishing and complementary machining). It can be seen that complementary machining has a similar level of high cycle fatigue strength as compared to shot peening. An examination of the complementary machining S-N curve shows an increase in the transition into low cycle fatigue ranges, and therefore, the transition into low cycle fatigue range can be compared to that achieved by the burnishing process. Contrary to this, no significant changes in fatigue strength are observed when comparing complementary machining to piezo peening. The piezo peening S-N curve

performs better in both the high and low cycle fatigue range. However, the primary disadvantage of these mechanical surface treatment methods is the requirement for an additional tool, which raises manufacturing costs and time. Given the ease of use and lack of extra equipment, the fatigue strength attained by complementary machining might be considered extraordinary in this respect.

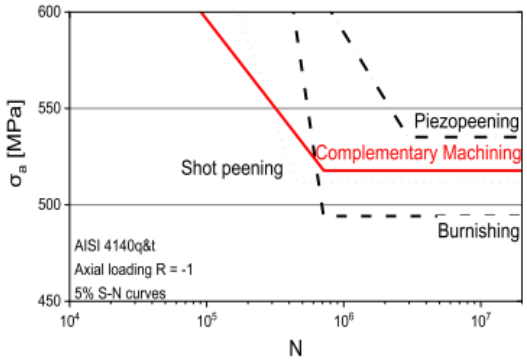

Figure 43. Comparison of AISI 4140 q&t 5% S-N curves; axial loading, stress ratio R = -1; processes: burnishing, shot peening, piezo peening, and complementary machining; based on [81].

2.4.5 Microstructure

The microstructure produced by AISI 4140's machining and complmentary machining was assessed by Gerstenmeyer et al. [78] (Figure 44).

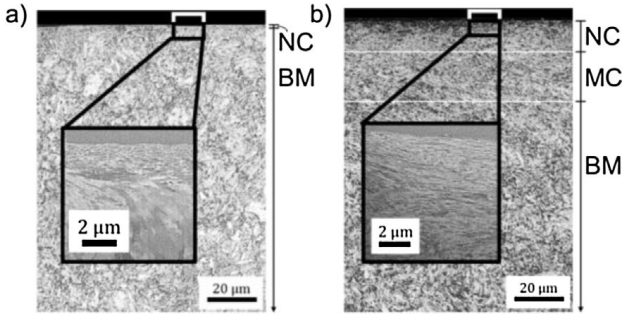

Figure 44. Microstructure (a) after machining and (b) after complementary machining using FIB technique and metallographic analysis [78].

Following machining, ne appreciable modifications were seen. Grain refinement at the surface layer was noted when the focused ion beam (FIB) technology was applied. A nanocrystalline surface layer with an average grain size of gs < 100 nm and an accomplished thickness of 1.68 µm was found when the FIB measurement was analyzed. A significant gradient of grain size characterizes the transition zone between the bulk material and the grain refined surface layer. According to Jawahir et al. [85], a surface layer that is impacted by machining is common, while the bulk material immediately beneath the surface layer is unaffected.

Following complementary machining, a much thicker grain refined surface layer was observed (Figure (44b)). The full thickness could not be measured with the FIB technique due to metrological limitations. The metallographic study was able to visualize the surface layer's microstructural alterations. Following complementary machining, the surface layer is characterized by a thick nanocrystalline layer down to 1.51 µm. A transition zone that is 20 meters thick comes next. A microcrystalline microstructure (MC, average grain size 0.1 < gs < 1 m) is discernible in the transition zone. The bulk material is obtained by taking into account these two surface layers. As previously mentioned in [60], the mechanical surface treatment procedure for orthogonal machining causes plastic deformation, which alters the surface layers' microstructure. Grain size changes up to the nanoscale occur when complementary machining is used in the turning process.

2.4.6 Residual stress

The effect of complementary machining on residual stresses and work hardening was examined by Gerstenmeyer et al. [78]. The X-ray diffraction method was used to assess residual stresses in accordance with the sin2φ approach [86]. Figure 45 displays the residual stress and work hardening findings. Tensile residual stresses over 430 MPa were attained at the surface for machining (Figure 45a). At a depth of z = 75 µm, the residual stresses in the farther course drop to at least -250 MPa. There was no discernible residual tension at a depth of z = 250 µm.

Surface tensile residual stresses persisted during machining regardless of lubricant use, most likely as a result of heat produced in the separation zone. The residual stress profile showed a similar tendency in both the axial and transverse directions. The surface experienced compressive residual pressures following complementary machining. A maximum of -1190 MPa was discovered for a depth of z = 20 µm, with residual stresses of -1066 MPa observed in the axial direction. At

a depth of z = 50 µm, these strong compressive residual stresses remain constant. As the distance from the surface grew, the compressive residual stresses dropped to 450 µm. At the surface, transverse residual stresses of -440 MPa were detected. For a depth of z = 250 µm, an increase in compressive residual stresses (-550 MPa) was observed; after this depth, the compressive residual stresses decreased and were eventually impossible to measure for a depth of z = 450 µm due to low surface treatment velocity, penetration depth, and lubrication use. Heat generation has no effect on the residual stresses. The workpiece's plastic deformation during the surface treatment procedure was blamed for the compressive residual stresses that were produced. For a depth of z = 250 µm in the transversal direction and z = 250 µm in the axial direction, these high compressive residual stresses are nearly linear. The residual stresses that occur are consistent with the findings of [81].

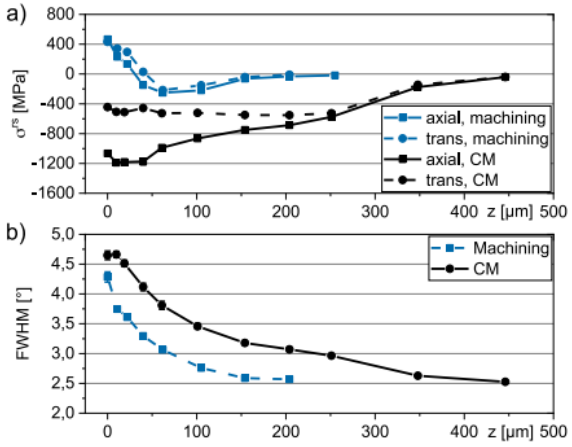

Figure 45. Residual stress (a), and work hardening (b) after machining and complementary machining [78].

The resulting work hardening after machining and complementary machining is shown in Figure 45(b). When evaluating the surface minimal differences between the component states were noticed. For both strategies, the work hardening is almost 4.5°, although the work hardening is a bit higher for complementary machining. The further courses of work hardening indicate a clear variation between the component states. After machining, at a depth of z = 150 µm, no changes in the work hardening occur at nearly 2.5°, which is in line with the residual stresses obtained (Figure 45(a)). After complementary machining, a larger depth effect of the work hardening was seen than from the machining process. An increase in depth resulted in a decrease in work hardening. This was in line with the results obtained from the residual stress observed in the transversal direction (Figure 45(b)), as the course decreased to a depth of z = 350 µm to a value of the work hardening of 2.5°.

3. Conclusion

The main findings from the work on complementary machining are as follows.

Complementary machining is more effective when conducted with a cooling lubrication system. Coated tools are appropriate for this process strategy, but the tool microgeometry significantly influences process sensitivity and the resulting surface layer states.

Because of the plastic deformation in the surface layer, complementary machining can produce grain refinement and minimize surface roughness. Surface roughness measurements Ra and Rz demonstrate this machining strategy's conditioning potential. Furthermore, the resulting roughness is significantly influenced by the velocity of surface treatment.

Cutting edge microgeometries with form-factors $K \geq 1$ are recommended for better results. Complementary machining can increase surface hardness HV, even in ductile materials. It can also achieve high compressive residual stresses.

Furthermore, complementary machining can significantly enhance fatigue limits compared to results after conventional machining. In comparison to the surface modification force F_{st}, the advanced microgeometry also significantly affects the passive force F_p.

Acknowledgments

The following individuals and organisations deserve special recognition:

1. For assistance and expertise, thank you to thesis supervisor Prof. R.F. Laubscher.
2. Prof. D.M. Madyira, for advice and direction during the study.
3. The University of Johannesburg, for the chance to learn at a prestigious institution.
4. The usage of resources and facilities by the Mechanical Engineering Department of the Faculty of Engineering and the Built Environmen

Competing Interest Statement

The authors declare no known competing financial interests or personal relationships that could have influenced the work reported in this paper.

Data and Materials Accessibility

All data generated or analysed during this study are included in this article.

Authors' Contributions

- Conceptualization: Author One and Two
- Methodology: Author One
- Investigation: Author One
- Discussion of results: Author One and Two
- Writing (original draft): Author One.
- Writing (review and editing): Author Two
- Approval of final text: Author Two

References

[1] H. Dagnall, Exploring Surface Texture, Leicester: Taylor Hobson Publishing Ltd, 1996.

[2] D. Whitehouse, Handbook of Surface Metrology, Bristol: Institute of Physics Publishing for Rank Taylor-Hobson Co.,, 1996.

[3] P. Benardos and G. C. Vosniakos, "Predicting Surface Roughness in Machining: A Review," *International Journal of Machine Tools and Manufacture,* vol. 43, no. 8, pp. 833-844, 2003.

[4] V. P. Astakhov, Surface Integrity – Definition and Importance in Function Performance, Michigan State : Department of Mechanical Engineering Michigan State University, 2010.

[5] B. Hudson, Surface Science − An Introduction, Boston: Butterworth-Heinemann, 1992.

[6] J. Riviere, Surface Analytical Techniques, Oxford: Oxford Science Publications, 1990.

[7] J. Walls, Methods of Surface Analysis: Techniques and Applications, New York: Cambridge University Press, 1992.

[8] P. Asthana, Micro-and Nano-Scale Experimental Approach to Surface Engineering Metals, in Mechanical Engineering, Taxes: Texas A&M University: College Station, 2006.

[9] C. Cotell, Preface, Surface Engineering, in ASM Handbook, Ohio: ASM International: Materials Park, 1994.

[10] R. King, "Chapter 1: Historical Background," in *Handbook of High-Speed Machining Technology*, New York, Chapman and Hall, 1985.

[11] Z. Peng, X. Zhang and D. Zhang, "Improvement of Ti–6Al–4V Surface Integrity through the use of High-speed Ultrasonic Vibration Cutting," *Tribology International,* vol. 160, 2021.

[12] M. Field and J. Kahles, "Surface Integrity - A new Requirement for Surfaces generated by Material Removal Methods," *DMIC Rep,* pp. 54-77, 1964.

[13] M. Field and J. Kahles, "Review of Surface Integrity of Machined Components," *CIRP,* vol. 20, no. 2, pp. 153-162, 1971.

[14] M. Field, J. Kahles and J. Cammett, "Review of Measuring Methods for Surface Integrity," *Annals CIRP,* vol. 21, no. 2, pp. 219-238, 1972.

[15] K. Tagazawa, "A Method of the Comprehensive Evaluation of Surface Integrity," *Manufacturing Engineering,* vol. 103, no. 1, pp. 51-57, 1989.

[16] D. U. T. Ozel, "Machining Induced Surface Integrity in Titanium and Nickel Alloys: A Review," *Internation Journal of Maching Tools and Manufacturing ,* vol. 51, pp. 250-280, 2011.

[17] D. Novovic, R. Dewes, D. Aspinwal, W. V. and P. Bowen, "The Effect of Machined Topography and Integrity on Fatigue Life," *International Journal of Maching Tools and Manufacturing,* vol. 44, no. 2-3, pp. 125-134, 2004.

[18] J. Kalisz, K. Żak, S. Wojciechowski, M. Gupta and G. Krolczyk, "Technological and Tribological Aspects of Milling-burnishing Process of Complex Surfaces," *Tribological International Journal,* 2020.

[19] A. Amanov, R. Karimbaev, E. Maleki, O. Unal, Y. Pyun and T. Amanov, "Effect of combined Shot peening and Ultrasonic Nanocrystal Surface Modification Processes on the Fatigue Performance of AISI 304," *Surface Coat Technology ,* vol. 358, pp. 695-705, 2019.

[20] V. Srinivasan and P. Palani, "Surface integrity, fatigue Performance and Dry Sliding Wear behaviour of Si3N4–TiN after wire-electro Discharge Machining," *Ceramic International ,* vol. 46, no. 8, pp. 10734-10739, 2020.

[21] C. Che-Haron and A. Jawaid, "The Effect of Machining on Surface Integrity of Titanium," *Jpurnal of Material Science and Process Technology,* vol. 166, pp. 188-192, 2005.

[22] J. S. Y. Guo, "A Comprehensive Experimental Study on Surface Integrity by End milling Ti–6Al–4V," *Journal of Material Science and Process Technology,* vol. 209, no. 8, pp. 4036-4042, 2009.

[23] X. Liang, Z. Liu and B. Wang, "State-of-the-art of surface Integrity Induced by Tool Wear Effects in Machining Process of Titanium and Nickel Alloys: A Review," *Measurement,* vol. 132, pp. 150-181, 2019.

[24] N. Khanna, C. Agrawal, M. Gupta and Q. Song, "Tool Wear and Hole Quality Evaluation in Cryogenic Drilling

of Inconel 718 Superalloy," *Tribological International Journal,* vol. 143, 2020.

[25] X. Liang and Z. Liu, "Tool wear behaviors and corresponding Machined Surface Topography during High-speed Machining of Ti-6Al-4V with Fine Grain Tools," *Tribological International Journal,* vol. 121, pp. 321-332, 2018.

[26] I. Jawahir, E. Brinksmeier, D. M. R M'Sauobi D.K Aspinwall J.C Outeir, D. Umbrello and A. Jayal, "Surface integrity in Metral Rermoval Processes: Recent Advances," *CIRP Annals,* pp. 603-626, 2011.

[27] V. Schulze, F. Bleicher, P. Groche, Y. Guo and Y. Pyun, "Surface Modification by Machine Hammer Peening and Burnishing," *CIRP Annals - Manufacturing Technology,* pp. 809-832, 2016.

[28] M. Torres and H. Voorwald, "An evaluation of Shot Peening, Residual Stress and Stress Relaxation on the Fatigue Life of AISI 4340 Steel," *International Journal of Fatigue,* vol. 24, pp. 877-886, 2002.

[29] K. Lu and J. Lu, "Nanostructured Surface Layer on Metallic Mterials Iuced by Suface Mechnical attrition Treatment," *Material Science and Engineering,* pp. 38-45, 2004.

[30] J. Gu, X. Wu, H. Cuypers and J. Wastiels, "Laser Shock Processing of Low Carbon Steel," *WIT Transc Engineering Science,* vol. 2, p. 14, 1998.

[31] J. Yang, Y. Her, N. Han and A. Clauer, "Laser Shock Peening on Fatigue Behavior of 2024-T3 Al Alloy with Fastener Holes and Stopholes," *Material Science and Engineering ,* vol. 298, pp. 296-299, 2001.

[32] W. Ting, L. Dongpo and G. Gang, "Investigations on the Nanocrystallization of 40Cr using Ultrasonic Surface Rolling Processing," *Applied Surface Science,* vol. 255, pp. 1824-1829, 2008.

[33] J. Liu, C. Ye and Y. Dong, "Recent Development of Thermally Assisted Surface Hardening Techniques: A Review," *Advances in Industrial and Manufacturing Engineering,* vol. 2, 2021.

[34] I. Horowitz, "Oberflachenbehandlung mittels Strahlmitteln Handbuch Uber Strahltechnik und Band 1: Die Grundlagen der Strahltechnik," vol. 1, 1982.

[35] J. Almen, "Peened Surface Improves Endurance of Machine Parts," *Metal Program,* pp. 209-315, 1943.

[36] J. Almen, "Shot Blasting to Increase Fatigue Resistance," *SAE Transactions,* pp. 248-268, 193.

[37] J. Frye and G. Kehl, "The Fatigue Resistance of Steel as Affected by some Cleaning Methods," *Transactions of ASM,* pp. 192-218, 1938.

[38] A. Gould and U. Evans, "The Effect of Shot-peening upon the Corrosion-fatigue of a High-carbon Steel," *Journal of the Iron and Steel Institute,* pp. 164-168, 1948.

[39] L. Tan, C. Yao, D. Zhang, J. Ren, X. Shen and Z. Zhou, "Effects of different Mechanical Surface Treatments on Surface Integrity of TC17 Alloys," *Surface and Coatings Technology,* vol. 398, 2020.

[40] Y. Liu, H. Li and M. Li, "Characterization of Surface Layer in TC17 Alloy Treated by Air Blast Shot Peening," *Materials,* vol. 65, pp. 120-126, 2015.

[41] L. Xie, C. Jiang and W. Lu, "The Influence of Shot Peening on the Surface Properties of (TiB + TiC)/Ti–6Al–4V," *Applied Surface Science,* vol. 280, pp. 981-988, 2013.

[42] L. Xie, Y. Wen, K. Zhan, L. Wang, C. Jiang and V. Ji, "Characterization on Surface Mechanical Properties of Ti–6Al–4V after Shot Peening," *Journal of Alloys and Compound,* vol. 666, pp. 65-70, 2016.

[43] D. Wu, C. Yao and D. Zhang, "Surface Characterization of Ti1023 Alloy Shot Peened by Cast Steel and Ceramic Shot," *Advanced Mechanical Engineering,* vol. 9, pp. 1-14, 2017.

[44] K. Li, X. Fu, R. Li, W. Zhou and Z. Li, "A mechanism study on Characteristic Curve of Residual Stress Field in Ti–6Al–4V Induced by Wet Peening Treatment," *Materials,* vol. 86, pp. 761-764, 2015.

[45] K. Li and G. C. W. Z. Z. L. X.S. Fu, "Mechanical Properties of Strengthened Surface Layer in Ti–6Al–4V Alloy Induced by Wet Peening Treatment," *Trans Nonferrous Metals Society China ,* vol. 26, pp. 2868-2873, 2016.

[46] N. Ao, D. Liu, X. Xu, X. Zhang and D. Liu, "Gradient nanostructure evolution and Phase Transformation of α Phase in Ti–6Al–4V Alloy Induced by Ultrasonic Surface Rolling Process," *Material Science and Engineering ,* vol. 742, pp. 820-834, 2019.

[47] Y. Ye, S. Kure-Chu, Z. Sun, X. Li, H. Wang and G. Tang, "Nanocrystallization and enhanced surface Mechanical Properties of Commercial Pure Titanium by Electropulsing-assisted Ultrasonic Surface Rolling," *Materials,* vol. 149, pp. 214-227, 2018.

[48] A. Bozdana and N. Gindy, "Comparative experimental Study on Effects of Conventional and Ultrasonic Deep Cold Rolling Processes on Ti–6Al–4V," *Material Science and Technology ,* vol. 24, pp. 1378-1384, 2008.

[49] A. Dekhtyar, B. Mordyuk, D. Savvakin, V. Bondarchuk, I. Moiseeva and N. Khripta, "Enhanced Fatigue behavior of Powder Metallurgy Ti–6Al–4V Alloy by Applying Ultrasonic Impact Treatment," *Material Science and Engineering ,* vol. 641, pp. 348-359, 2015.

[50] C. Liu, D. Liu, X. Zhang, D. Liu, A. Ma, N. Ao and X. Xu, "Improving Fatigue Performance of Ti–6Al–4V Alloy via Ultrasonic Surface Rolling Process," *Journal of Material Science and Technology ,* vol. 35, pp. 1555-1562, 2019.

[51] X. Zhao, G. Xue and Y. Liu, "Gradient crystalline structure induced by Ultrasonic Impacting and Rolling and its Effect on Fatigue behavior of TC11 Titanium Alloy," *Results Physics,* vol. 7, pp. 1845-1851, 2017.

[52] X. Nie, W. He, S. Zang, X. Wang and J. Zhao, "Effect study and application to improve High Cycle Fatigue Resistance of TC11 Titanium Alloy by Laser Shock Peening with Multiple Impacts," *Surface Coating Technology,* vol. 253, pp. 68-75, 2014.

[53] X. Nie, W. He, L. Zhou, Q. Li and X. Wang, "Experiment Investigation of Laser Shock Peening on TC6 Titanium Alloy to Improve High Cycle Fatigue Performance," *Material Science and Engineering,* vol. A, no. 594, pp. 161-167, 2014.

[54] C. Cellard, D. Retraint, M. François, E. Rouhaud and D. L. Saunier, "Laser Shock Peening of Ti-17 Titanium Alloy: Influence of Process Parameters," *Material Science and Engineering,* vol. A, no. 532, pp. 362-372, 2012.

[55] S. Zou, J. Wu, Y. Zhang, S. Gong, G. Sun, Z. Ni, Z. Cao, Z. Che and A. Feng, "Surface Itegrity and Fatigue Lves of Ti17 Cmpressor Bades Sbjected to Lser Sock Pening with Suare Sots," *Surface Coating Technology ,* vol. 347, pp. 398-406, 2018.

[56] H. Qiao, "Experimental Investigation of Laser Peening on Ti17 Titanium Alloy for Rotor Blade Applications," *Applied Surface Science,* vol. 351, pp. 524-530, 2015.

[57] O. Foppl and G. v. Heydekampf, "Dauerfestigkeit und Konstruktion," *Manufacturing Sceince and Technology,* vol. 45, pp. 1087-1094, 1929.

[58] A. Thum and H. Wiegand, "Die Dauerhaltbarkeit von Schraubenverbindungen und Mittel zu ihrer Steigerung," *Verein Deutscher Inenieure,* pp. 1061-1063, 1933.

[59] J. Schwalm, M. Gerstenmeyer, F. Zanger and V. Schulze, "Complementary Machining: Effect of Tool Types on Tool Wear and Surface Integrity of AISI 4140," *Procedia CIRP ,* pp. 89-94, 2020.

[60] F. Zanger, M. Gerstenmeyer and H. Weule, "Identification of an Optimal Cutting Edge Microgeometry for Complementary Machining," *CIRP Annals - Manufacturing Technology,* vol. 66, pp. 81-84, 2017.

[61] I. Kharapur, "Geometry of Single Point Cutting Tool," NPTEL, 2011. [Online]. Available: https://nptel.ac.in/courses/112105127/pdf/LM-03.pdf. [Accessed 15 May 2019].

[62] A. N. Standard, "Basic Nomenclature and Definitions for Single - Point Cutting Tools," The American Society of Mechanical Engineers , New York, 1995.

[63] ". 3002/1-1982, "Basic Quantities in Cutting and Grinding- Part 1: Geometry of the Active Part of Cutting Tools – General Terms Reference Systems, Tool and Working Angles, Chip Breakers," International Standard Organization,, 1982.

[64] S. Odelros, "Tool Wear in Titanium Machining," Uppsala Universitet, Uppsala, 2012.

[65] S. .. Rewatkar, N. .. Deshbhratar, A. .. Kawale, A. .. Kardam and A. .. Naik, "Review of Influence Of Different Cutting Angles of Single Point Cutting Tool on Turning Operation," *International Research Journal of Engineering and Technology,* vol. 4, no. 2, 2017.

[66] "Single Point Cutting Tool: Nomenclature and Tool Signature," ME Mechanical, 17 April 2019. [Online]. Available: https://me-mechanicalengineering.com/single-point-cutting-tool/. [Accessed 15 May 2019].

[67] J. Fulemova and J. Rehof, "Influence of Form Factor of the Cutting Edge on Tool Life during Finishin Milling," *Procedia Engineering,* vol. 100, pp. 682-688, 2014.

[68] B. Denkena, J. Kohler and M. Mengesha, "Influence of the Cutting Edge Rounding on the Chip Formation Process: Part1. Investigation of Material Flow, Process Forces and Cutting Temperature," *Production Enginerring,* vol. 6, no. 4-5, pp. 329-338, September 2012.

[69] B. Denkena, J. Kohler and C. Venturn, "Customized Cutting Edge Preparation by Means of Grinding," *Precision Engineering,* vol. 37, no. 3, pp. 590-598, July 2013.

[70] B. Denkena, E. Bassett and J. Kohler, "On the Honed Cutting Edge and its Side Effects durinf Orthogonal Turning Operations of AISI1045 with Coated WC-Co Insters," *CIRP Journal of Manufacturing Science and Technology,* vol. 5, no. 2, pp. 108-126, 2012.

[71] C. Wyen and K. Wegener, "Influence of Cutting Edge Radius on Cutting Forces in Machining of Titanium," *CIRP Annals - Manufacturing Technology,* vol. 59, no. 1, pp. 93-96, 2010.

[72] B. Denkena, J. Köhler, B. Breidenstein, A. Abrão and C. Ventura, "Influence of the Cutting Edge Preparation Method on Characteristics and Performance of PVD Coated Carbide Inserts in Hard Turning," *Surface & Coatings Technology,* vol. 254, p. 447–454, 2014.

[73] H. Puls, F. Klocke and D. Lung, "A New Experimental Methodology to Analyse the Friction behaviour at the Tool-chip Interface in Metal Cutting," *Production Engineering,* vol. 6, pp. 349-34, 2012.

[74] H. Puls, F. Klocke and D. Lung, "Experimental Investigation of Friction Metal Cutting Conditions," *Wear,* vol. 310, pp. 63-71, 2014.

[75] E. Segebade, F. Zanger and V. Schulze, "Influence of Different Asymmetrical Cutting Edge Microgeometries on Surface Integrity," *Procedia CIRP,* vol. 45, pp. 11-14, 2016.

[76] M. Gerstenmeyer, B.-L. Ort, F. Zanger and V. Schulze, "Influence of the Cutting Edge Microgeometry on the Surface Integrity during Mechanical Surface Modification by Complementary Machining," *Procedia CIRP,* vol. 58, pp. 55-60, 2017.

[77] M. Gerstenemyer, F. Zanger and S. Volker, "Complementary Machining – Machining Strategy for Surface Modification," *Procedia CIRP,* vol. 45, pp. 247-250, 2016.

[78] M. Gerstenmeyer, F. Zanger and V. Schulze, "Influence of Complementary Machining on Fatigue Strength of AISI 4140," *CIRP Annals - Manufacturing Technology,* vol. 67, pp. 583-586, 2018.

[79] D. E. NORM, "GPS – Surface Texture: Profile Method Rules- DIN_EN_4288_1998," June 1982. [Online]. Available: https://kupdf.net/download/din-en-4288-

1998-pdf_58cbd467dc0d608529c3464d_pdf. [Accessed 27 October 2021].

[80] J. Fulemova and Z. Janda, "Influence of the Cutting Edge Radius and Cutting Edge Preparation on Tool Life and Cutting Forces at Inserts with Wiper Geometry," *CIPC,* vol. 69, pp. 565-573, 2014.

[81] F. Lienert, J. Hoffmeister, A. Erz and V. Schulze, "Influence of Piezo Peening on the Fatigue Strength of Quenched and Tempered AISI 4140," *International Scientific Committee for Shot Peening 12,* 2015.

[82] F. Zanger and M. Gerstenmeyer, "Materials Behaviour of Armco-Iron and AISI 4140 at High Speed Deformation dueing Machining," *Advance Materials Research,* vol. 1018, pp. 161-166, 2014.

[83] V. Schulze, J. Michna, F. Zanger and R. Pabst, "Modeling the Process-induced Modifications of the Microstructure of Workpiece Surface Zones in Cutting Processes," *Advanced Materials Research,* vol. 380, pp. 233-371, 2011.

[84] H. Puls, F. Klocke and D. Lung, "A New Experimental Methodology to Analyse the Friction behaviour at the Tool-chip Interface in Metal Cutting," *Process Engineering Research Development,* vol. 6, pp. 349-354, 2012.

[85] E. Brinksmeier, R. M'Saoubi, D. Aspinwall, J. Outeiro, D. Meyer, D. Umbrello and A. Jayal, "Surface Integrity in Material Removal Processes: Recent Advances.," *CIRP Annals — Manufacturing Technology,* vol. 60, no. 2, pp. 603-626, 2011.

[86] E. Macherauch and P. Müller, "The sin2 Method of Radiographic Voltage Measurement," *Journal of Applied Physics,* vol. 13, pp. 305-312, 1961.